PŘÍRODOVĚDECKÁ FAKULTA UNIVERZITY
PALACKÉHO V OLOMOUCI

SPOLEČNÁ LABORATOŘ OPTIKY

Kvantové a klasické strojové učení pro kvantově informační protokoly

Autoreferát

Jan Roik

školitel

doc. Mgr. Karel Lemr, Ph.D.

OLOMOUC 6. března, 2023

Název práce	Kvantové a klasické strojové učení pro kvantově informační protokoly
Uchazeč	Mgr. Jan Roik
Školitel	doc. Mgr. Karel Lemr, Ph.D.
Oponenti	

Obhajoba proběhne dne ..... 2023 v ..... hodin před komisí pro obhajobu disertační práce, studijního oboru Nanotechnologie na katedře Společné laboratoře optiky Univerzity Palackého v Olomouci sídlící na adrese třída 17. listopadu 50A, 772 07 Olomouc.

Disertační práce je dostupná k nahlédnutí na studijním oddělení Přírodovědecké fakulty Univerzity Palackého v Olomouci sídlící na adrese třída 17. listopadu 1192/12, 779 00 Olomouc.

Contents

Chapter 1

Introduction

The presented thesis was written with the intention to summarize and consolidate the authors' published research focused on the potential of machine learning in quantum information processing. The research was carried out at the Joint Laboratory of Optics, Palacký university and Institute of Physics of Academy of Sciences of the Czech Republic[1]. This research facility offered decades of collective experiences in quantum information processing and machine learning [1–3]. The author also collaborated with theoreticians from the University of Adam Mickiewicz in Poznan[2].

Foundings presented in Chapters 3–5 are adopted from authors' journal publications containing the original results. Declarations of author's contribution are attached in the Appendix.

Accuracy of entanglement detection via artificial neural networks and human-designed entanglement witnesses

Based on Author's publication: J. Roik, K. Bartkiewicz, A. Černoch, and K. Lemr Physical Review Applied, vol. 15, no. 5, p. 054006, 2021 [A-1].

Quantum entanglement is one of the most intriguing phenomena ever discovered by humankind. It has become a cornerstone for many applications, such as quantum cryptography [4], superdense coding [5], teleportation [6], and quantum computation [7]. Therefore it is essential to know how to distinguish entangled states. However, even nowadays, we still lack efficient and general methods to do so.

[1] 17. listopadu 50A, 772 07 Olomouc, Czech Republic
[2] Uniwersytetu Poznańskiego 2, 61-614 Poznań, Poland

Currently, the most popular methods are full-state tomography and entanglement witnesses. Unfortunately, neither of them is optimal. Full-state tomography offers a complete quantum state description but is experimentally demanding and scales undesirably with the complexity of the investigating state. On the other hand, prominent entanglement witnesses such as collectibility [8], Clauser, Horne, Shimony, Holt (CHSH) nonlocality [9], fully entangled fraction [10], and entropy witnesses [11] do not guarantee correct classification of the investigated state. The idea of using a neural network to classify entangled states was initially demonstrated by Gao *et al.* in 2018 [12]. However, they considered only entangled linear witnesses, which allowed them to classify only a limited class of states.

Under those presumptions, we set our research goal to use the artificial neural network as the nonlinear entanglement witness, aiming to maximize the classification success rate for all general two-qubit stats while reducing required resources. The neural network performance was compared against the prominent analytical witnesses for random general 2-qubit quantum states.

Entanglement quantification from collective measurements processed by machine learning

Based on Author's publication: J. Roik, K. Bartkiewicz, A. Černoch, and K. Lemr, Physics Letters A, vol. 446, p. 128270, 2022 [A-2].

The promising performance of the artificial neural network to detect entangled states demonstrated in prior research [A-1] has motivated us to extend our effort to a more general task. This follow-up research aimed not only to classify general two-qubit states but quantify them, i.e., determine their degree of entanglement. Conventionally, one must perform full state tomography to reconstruct the investigated state's density matrix and subsequently calculate entanglement measures [13], which both scales unfavorably with the complexity of investigated state.

The research goal was to employ the artificial neural network to reduce the number of projections required for accurate entanglement quantification based on the results of collective measurement using a minimal set of tomographic projections [14]. We investigated correlations between the precision of the quantification as a function of the measurement configuration. The investigation was carried out on the general two-qubit states, and the negativity was used as an entanglement quantifier [15]. In the end,

the performance of the artificial neural network was benchmarked against the capabilities of the polynomial regressions method.

Routing in quantum communications networks using reinforcement machine learning

Based on Author's publication: J. Roik, K. Bartkiewicz, A. Černoch, and K. Lemr, submitted (2023) [A-3].

With the recent evolution of quantum technologies, concepts such as the large-scale quantum networks "quantum internet" are steadily becoming a reality. Although we have already overcome many obstacles, few remain unaddressed [16]. One of the most crucial is identifying an effective protocol for route-finding in a teleportation-based quantum network [17]. The quantum nature of these networks introduces properties unique to the quantum world, such as non-additive noise (amplitude dumping [18], correlated phase noise [19]). Non-additive noise is the main reason we cannot simply use classical graph path and tree-finding algorithms because they cannot handle non-additivity, which often leads to suboptimal solutions.

In order to maintain stable and safe communication, one needs to use as error free roads as possible (i.e., find the optimal solution). Therefore, we focused our research efforts on identifying the protocol capable of route-finding in a quantum network, emphasizing the maximization of the entangled fraction between the shared state.

In our research, we promote reinforcement learning represented by the proximal policy optimization (PPO) algorithm [20] as an efficient solution to the outlined problem. This algorithm was benchmarked against the Monte-Carlo search. We demonstrate the performance of both algorithms on various scenarios set in the quantum network. [3]

[3] Topology was inspired by one of the possible topologies of 6G networks [21].

Chapter 2

Accuracy of entanglement detection via artificial neural networks and human-designed entanglement witnesses

Text adopted from *Jan Roik, Karol Bartkiewicz, Antonín Černoch, and Karel Lemr, Physical Review Applied, vol. 15, no. 5, p. 054006, 2021* [A-1].

2.1 Introduction

Quantum entanglement is an intriguing phenomenon described almost a century ago by Schrödinger, Einstein, Podolsky, and Rosen [22, 23]. Since then many theoretical and practical papers alike, as well as vivid discussions, were dedicated to this topic [24–26]. The ability to effectively detect entangled state became essential mainly because of their application potential in quantum computing [27], quantum cryptography [4], and quantum teleportation experiments [28]. The most robust way of detecting it is via a full state tomography and density matrix estimation [29]. This method allows us to obtain all information about the state and thus correctly detect entanglement. Unfortunately this method is experimentally demanding because the number of required projections grows exponentially with the dimension of Hilbert space. There is also a variety of other methods that do not rely on full-state tomography [9, 30–49]. These methods include a

wide range of linear entanglement witnesses [30–35] of the CHSH- Clauser Horne Shimony Holt type [9]. While for pure states, these methods give similar results, their outcomes might vary significantly when mixed states are considered. While requiring only a relatively few measurement configurations, these witnesses can not reliably function without some a prior information about the detected state. To circumvent this limitation, while not resorting to state tomography, non-linear entanglement witnesses have been proposed.

In 2011, Rudnicki *et al.* introduced a nonlinear entanglement witness called *Collectibility* [43, 45]. For a visual demonstration of this concept [see Fig. 2.1 a)]. For 2-qubit states, this witness requires two simultaneously prepared copies of the investigated state. Then a Bell state projection is imposed on a pair of corresponding qubits from each copy and the remaining qubits are subjected to local measurements. For a general 2-qubit state, this requires a combination of 5 local projections and, thus, fewer measurement configuration than full quantum state tomography which includes at least 24 projections. One can further decrease the time needed for a QST if measurements can be performed in parallel on multiple copies of the investigated state. When dealing with unknown quantum states, collectibility can detect a much broader range of states compared to linear witnesses. Namely, it detects all pure entangled states. Unfortunately, it detects entanglement of only a fraction of mixed states. This shortcoming is characterized by a rather big Type-II error (false negative), as we show later. On the other hand, all states which are classified as entangled by this method are classified correctly (Type-I error is null, there are no false-positive classifications). We demonstrate that significant improvement can be reached when collective entanglement witnesses are devised using an artificial neural network. As demonstrated by Gao *et al.* [12] and other groups [50, 51], neural networks can be used to identify quantum states. However, only linear entanglement witnesses were considered which significantly limited the class of detected entangled states. Note that neural network-based linear witnesses share the same shortcomings with their analytical counterparts, which is the need for a prior information about the investigated state.

We train a neural network to classify quantum states by providing it with results of collective measurements and demonstrate its significantly better performance over collectibility and other similar non-linear witnesses for a general 2-qubit state as well as for real experimental data for a fixed number of measurement configurations. Moreover, we show the

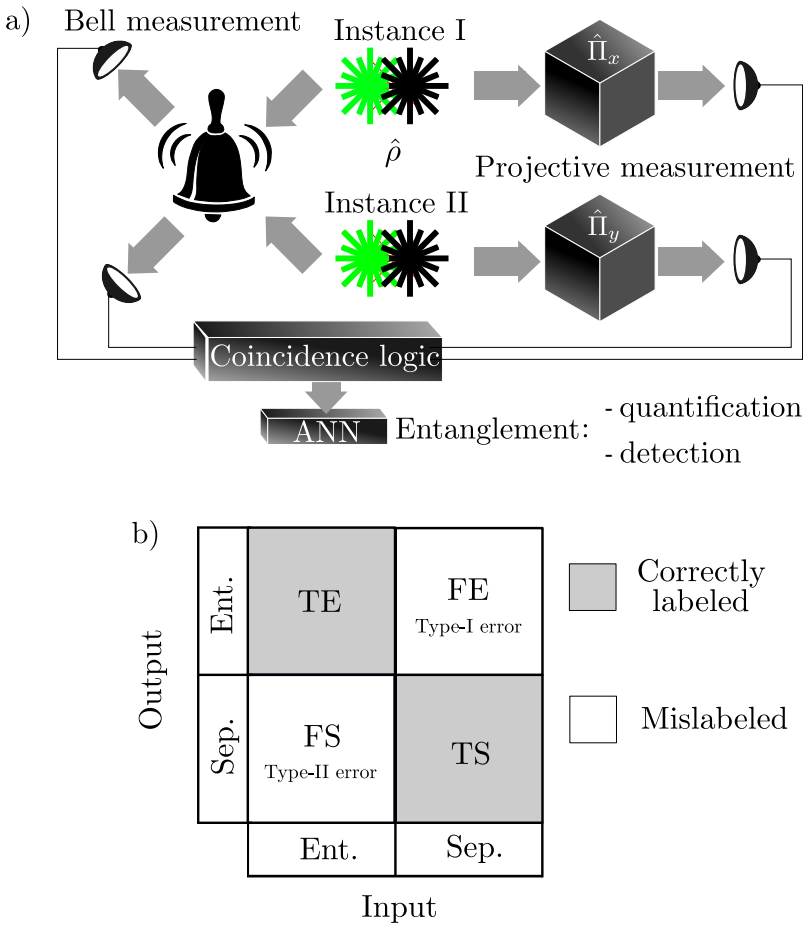

Figure 2.1: a) Scheme of a collective measurement: two instances of the investigated states $\hat{\rho}$ are subject to simultaneous measurement. While one qubit of each instance undergoes local projections, the other two qubits are nonlocally projected onto a Bell state. These coincidence detections can be fed to an artificial neural network that can serve as an entanglement witness or even entanglement quantifier (measure) for investigated state $\hat{\rho}$. b) Schematic depiction of the confusion matrix used for performance evaluation of the ANN. TE - truly entangled, FE - falsely entangled, TS - truly separable, FS - falsely separable, Sep. - separable, Ent. - entangled.

increasing capability of the neural network when provided with a larger amount of measurement configuration outcomes by comparing it against three other analytical methods that require 12 projections, namely FEF – fully entangled fraction [10,52,53], CHSH [9], and entropic witness [11,54]. We use confusion matrix as a method of performance evaluation for the ANN and previously known non -linear witnesses [see Fig. 2.1 b)]. Diagonal elements show the number of correctly labeled input states TE - truly entangled and TS - truly separable furthermore off-diagonal elements provide information about falsely labeled input states FE - falsely entangled and FS - falsely separable.

2.2 Collective measurements

Although our idea can be generalized, we focus our investigation on the entanglement of two-qubit states $\hat{\rho}$. In order to perform collective measurements on these states, one needs to start with the preparation of two instances of $\hat{\rho}$ resulting in an overall density matrix of the entire system $\hat{\rho}_4 = \hat{\rho} \otimes \text{SWAP}\ \hat{\rho}\ \text{SWAP}^\dagger$; where the SWAP operator interchanges the order of subsystems. One qubit from each instance is projected locally, while the remaining qubits undertake a nonlocal Bell-state projection. For the visualization of this procedure, see Fig. 2.1 a). For a given pair of local projections, the result of collective measurement is the probability of a successful singlet Bell-state projection imposed on the nonlocally projected qubits

$$P_{xy} = \frac{\text{Tr}[(\hat{\rho}_4)\,(\hat{\Pi}_x \otimes \hat{\Pi}_{\text{Bell}} \otimes \hat{\Pi}_y)]}{\text{Tr}[(\hat{\rho}_4)\,(\hat{\Pi}_x \otimes \hat{\mathbb{1}}^{(4)} \otimes \hat{\Pi}_y)]}. \tag{2.1}$$

In this equation $\hat{\Pi}_x$ and $\hat{\Pi}_y$ are local projections onto single-qubit states $|x\rangle$ and $|y\rangle$, $\hat{\Pi}_{\text{Bell}}$ denotes projection onto the singlet Bell state and $\hat{\mathbb{1}}^{(4)}$ represents four-dimensional identity matrix [43]. One collective measurement configuration corresponds to the choice of one $\hat{\Pi}_x$ and one $\hat{\Pi}_y$. Obtained set of B probabilities[1] $P_{xy}^{(i)}\,; i = 1,...,B$ is subsequently fed to a neural network for training together with labels obtained by the PPT- Peres-Horodecki criterion [55, 56].

[1] In the original paper referred to as N here relabeled to avoid confusion with Negativity.

2.3 Artificial neural network

TensorFlow 2.0 [57] was used to program a neural network capable of classifying quantum states. We experimented with the complexity of the network and our final layout of the network with 5 hidden layers containing $36, 180, 75, 180,$ and 75 nodes respectively seems to be the optimal choice to find a balance between obtained precision and computation time. The proposed network is capable of assigning any quantum state with a value $w \in [0;1]$ which can be interpreted as a confidence factor from 0 (certainly entangled) to 1 (certainly separable). We defined decision threshold ϵ to convert the w values to a binary label: $w < \epsilon \Rightarrow$ entangled, $w \geq \epsilon \Rightarrow$ separable. By changing ϵ value we make the network biased towards the desired decision which allowed us to tune the trade-off between Type-I and Type-II errors. The network was trained on 4×10^6 samples and tested on the other 4×10^5 samples with distribution containing 67.74% entangled states and 32.26% separable states. The main goal was to test the network against collectibility, therefore, we start to train it using the same $B = 5$ projection settings. In the next step, we also tested capability of the network for $B = 3, 6, 12, 15$ projection settings.

2.4 Results

In the first step, we decided to test the neural network with decision threshold $\epsilon = 0.5$ for a several amounts of projection settings $B = 3, 5, 6, 12, 15$. As it turns out the neural network was capable of labeling entangled and separable states even using 3 projection settings with an overall success rate of around 83.33%. For an increasing number of projection settings success rate increased even further and reached 96.55% for 15 projections settings. We plot the probability of incorrect decision as a function of the smallest eigenvalue of the partially transposed density matrix $\hat{\rho}$ (see Fig. 2.2).

As expected, the neural network struggles with the states close to the PPT decision boundary (minimal eigenvalue close to zero). Unfortunately, the neural network is, to some extend, prone to Type-I errors (separable state classified as entangled). As it turns out the network is more likely to make a mistake when classifying separable states than entangled states. Our solution is to change the decision threshold ϵ to decrease the Type-I error. This means that we demand more certainty from the network when classifying the entangled state. By optimizing thresholds we manage to find the value which satisfies a condition of Type-I error $< 1\%$ which we find

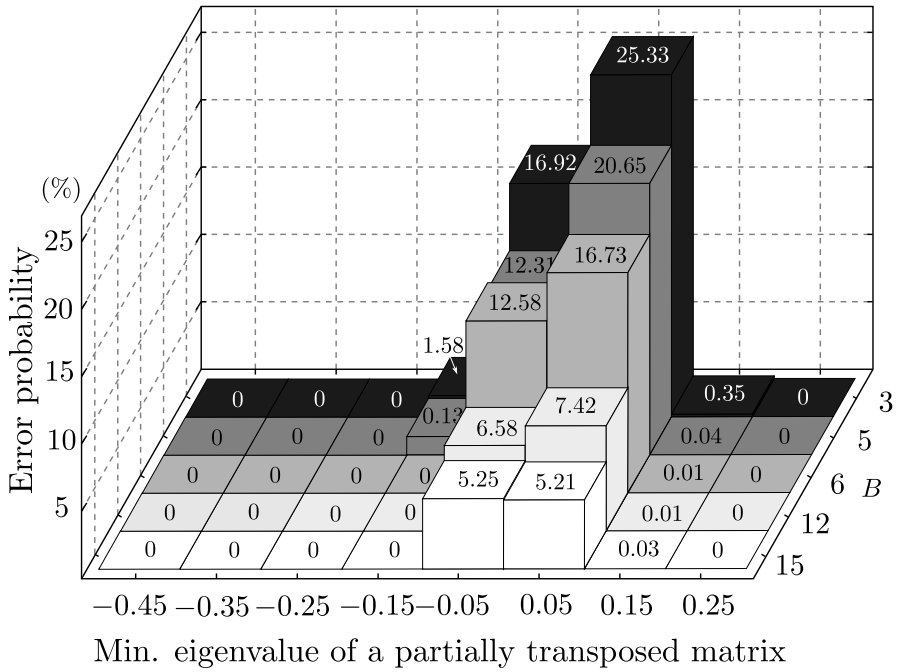

Figure 2.2: The result obtained by the neural network with decision threshold $\epsilon = 0.5$ for $B = 3, 5, 6, 12, 15$ and distribution containing 67.74% entangled states and 32.26% separable states. In this graph probability of false prediction is plotted against the minimal eigenvalue of a partially transposed matrix.

acceptable. It is possible to arbitrarily decrease the Type-I error by sacrificing the detection capability characterized by Type-II error. For more detailed dependence of Type-I and Type-II error on threshold for $B = 3, 5, 6, 12, 15$ see Fig. 2.3. In the next step we compared the network performance against collectibility. The neural network fed by outcomes of the same 5 projection settings also required by the collectibility was able to correctly classify 78.14% of all states while committing Type-I error of 0.96% ($\epsilon = 0.9$). This performance vastly surpassed the capability of the Collectibility which identifies only 36.59% of the states correctly (see Tab. 2.1). To further highlight the potential of ANN we compared its performance with analytical methods (FEF, CHSH, and EW) (see Tab. 2.1). The success rate of the ANN surpass capabilities of FEF by 6.01%, EW by 34.01%, and CHSH by 46.01% while committing Type-I error 0.24%. This means that if we can accept

	ANN				
B	3	5	6	12	15
Type-I error (%)	0.93	0.96	1.18	0.24	0.22
Type-II error (%)	33.47	20.91	15.88	7.74	5.24
Success rate (%)	65.50	78.14	82.94	92.01	94.54

	Collectibility	FEF	EW	CHSH
B	5	12	12	12
Type-I error (%)	0	0	0	0
Type-II error (%)	63.41	14.00	42.00	54.00
Success rate (%)	36.59	86.00	58.00	46.00

Table 2.1: Comparison of the results obtained by ANN for $B = 3,5,6,12,15$ with prominent analytical methods (collectibility, FEF - fully entangled fraction, EW - entropic witness, CHSH nonlocality). Both Type-I and Type-II errors are taken for decision threshold $\epsilon = 0.9$ to ensure Type-I error < 1%.

some Type-I error, it is possible to achieve a major improvement in entangled states detection using the neural network. Note that the purpose of this research was not to use ANN simply to fit existing entanglement witnesses, but rather to devise completely new ones that we later compare with these already known analytical formulas.

We have investigated the possibility to derive approximate analytical formulas from the parameters of trained ANNs. This is a rather complex task and we were only able to find a reasonable formula for $B = 3,5$ measurement configurations. Using logistic regression, a witness in the form of

$$W_B = \left[1 + \mathrm{e}^{-z_B}\right]^{-1}, \tag{2.2}$$

where $z_B = \vec{w}_B \cdot \vec{p}_B$ and $\vec{p} = (1, P_{HH}, P_{VV}, P_{HV}, P_{DD}, P_{AA})$ for $\vec{w}_3$ = (-2.3348, 19.3139, 21.5486, -11.4228, 0, 0) and $\vec{w}_5$ = (0.0009, 7.7967, 9.6227, -25.8294, 21.9 635, 22.0167) can be obtained. The states for which $W_B < 0.05$ are classified as entangled (separable otherwise). This decision boundary implies Type-I error of circa 0.9% and Type-II errors of 57.5% and 44.8% corresponding to $B = 3,5$ respectively. Type-I errors can be made arbitrary small by lowering the threshold value of W_B for classifying a given state as entangled.

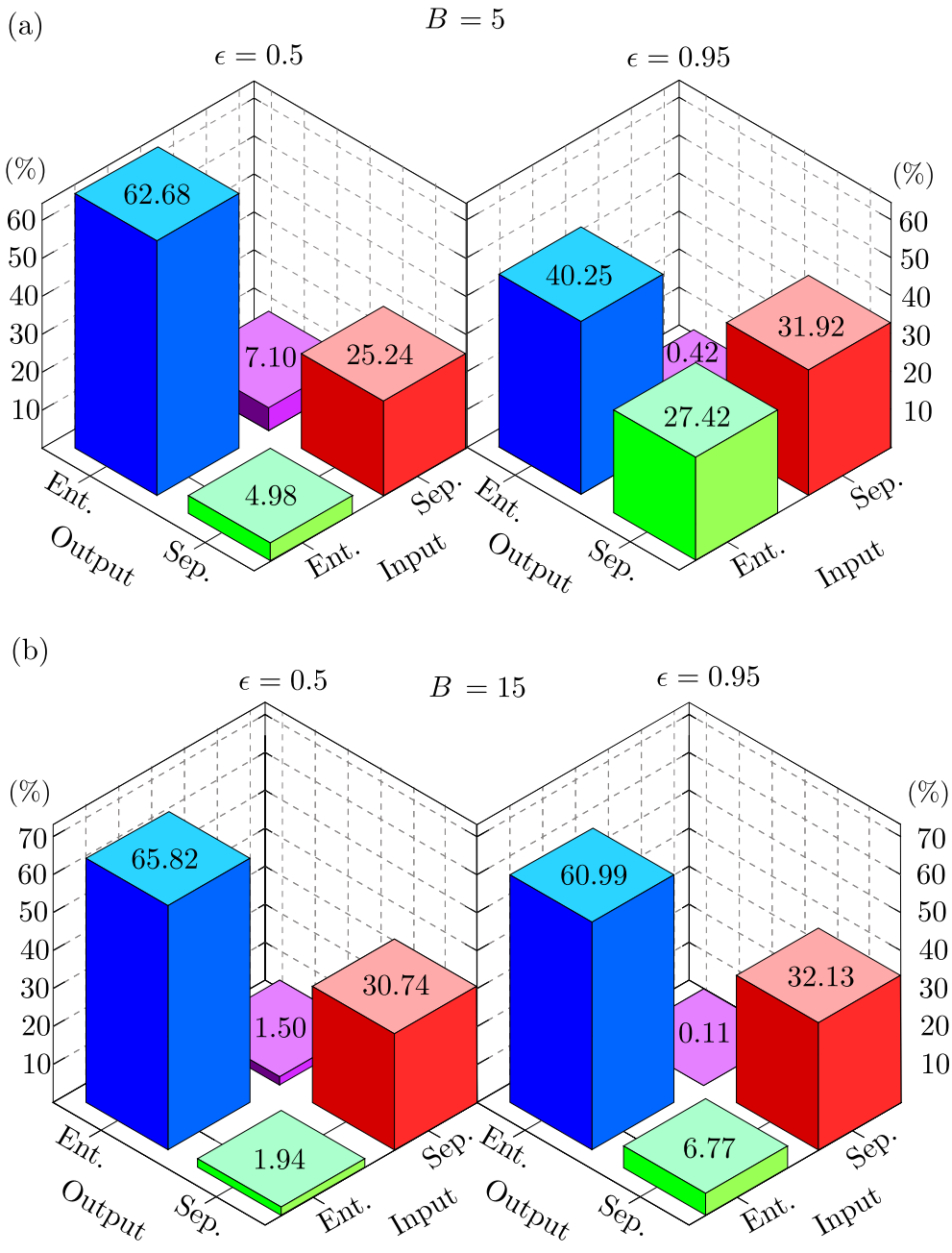

Figure 2.3: Performance dependence of the ANN on decision threshold ϵ = 0.5, 0.95 with distribution containing 67.74% entangled states and 32.26% separable states depicted as confusion matrices for: a) $B = 5$; b) $B = 15$.

2.5 Experimental implementation

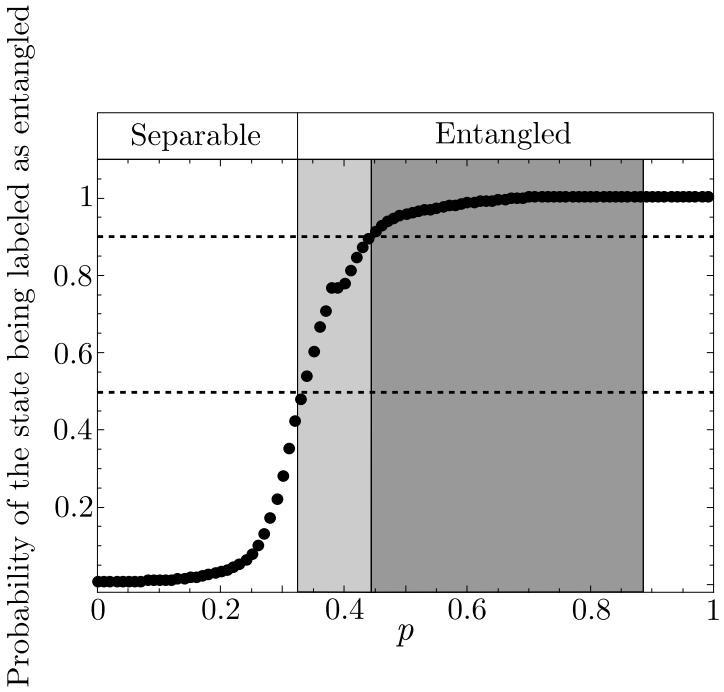

Figure 2.4: Results obtained by neural network and collectibility respectively from a real experimental data set $B = 5$. Black full dots show the probability of a Werner state being labeled as entangled by the ANN. The light-gray area covers the values of p which neither the neural network nor collectibility can classify correctly. The dark-gray area represents the range of p values for which the ANN classifies the Werner states correctly and collectibility fails. The dashed lines represent the decision thresholds $\epsilon = 0.9$ and 0.5 respectively.

To verify the network capability we decided to further test it on a set of real experimental data. For this purpose, we used the data set from the first-ever Collectibility measurement from 2016 [58]. In that particular experiment, a class of Werner states of the form of $\hat{\rho}_w = p|\psi^-\rangle\langle\psi^-| + (1-p)\hat{\mathbb{1}}/4$, was investigated. $|\psi^-\rangle$ represents singlet Bell state, and $\hat{\mathbb{1}}/4$ stands for the maximally mixed state. We set the detection threshold to $\epsilon = 0.9$ like in the previous comparisons of the neural network with collectibility, to be con-

sistent and make test conditions as fair as possible. Results show that collectibility can classify states with $p > 0.89$ as entangled witch corresponds with its theoretical prediction. The neural network, on the other hand, detects entangled states when $p > 0.44$ (see Fig. 2.4). Note that it is known that Werner states are entangled for $p > \frac{1}{3}$.

2.6 Conclusions

We trained a neural network to classify general qubit states based on nonlinear collective witnesses. Our main goal was to compare the capability of this network against a prominent analytical representation of nonlinear witnesses: the collectibility. The network can classify the general two-qubit states significantly more efficiently than collectibility with Type-I error $< 1\%$. The ANN also surpasses FEF, CHSH, and entropic witness when taught on 12 projections (the same amount needed by the mentioned analytical witnesses). Increasing the number of projection settings improves the ANN's decision even more. We further support this claim by using the network on a real experimental data set. The network confirmed its potential by correctly labeling a broad range of states where collectibility fails. Moreover, it achieved a Type-I error $= 0$ on Werner states. Our research promotes the idea of using artificial intelligence towards a better understanding of the intriguing physical phenomena such as the entanglement. We have demonstrated that the neural network can quickly train to become a valid efficient collective entanglement witness. We have directly compared its performance with analytical formulas. Using nonlinear measurements (on two copies of the state), our network operates completely free of any a priory information that can bias comparison of its performance with analytical counterparts. Moreover, we have shown that the training performed on numerically generated states works very well on real experimental data corresponding to states completely unknown to the ANN.

Because of technical limitations on the possible complexity of our ANN and on the number of samples processed in ANN training, reaching the limit of zero Type-I error was not possible. However, we were able to tune this error to a fraction of a percent by choosing a proper value of ϵ. By extrapolating our results for the whole available range of ϵ, we conclude that the limit of vanishing Type-I error is reached by the ANN for $\epsilon = 0.9822$ and $\epsilon = 0.9994$ for 5 and 12 measurements, respectively. The Type-II errors for these values of ϵ are 31.26% (5 measurements, about 32% better then col-

lectibility) and 11.40% (12 measurements, 2.6% better than FEF). Thus, we have demonstrated that the best known analytical methods for certifying entanglement with a few measurements can be further improved. Notably, the 2.6% smaller Type-I error of ANN with respect to FEF, means that ANN fails relatively on about 20% less states than FEF using the same input. This demonstrates that there is still a place for improvement in the theory of experimentally-friendly entanglement detection. The extrapolation of functional the dependence of Type-I and II errors on ϵ was performed by fitting a quadratic and an exponential curve, respectively. We believe that the high quality of both fits and the proximity of the lowest Type-I error data point to 0 justify our conclusions. We hope that our results will stimulate further research in experimentally-friendly methods of classifying quantum states.

Further to that, the theoretical assumption of zero Type-I error of analytical witnesses does not hold operationally because of unavoidable experimental imperfections and finite precision of all measurements. As a result, separable states close to the decision boundary may be misclassified even using theoretically infallible witnesses. In this study, we have allowed the ANN a Type-I error of about 1% which we believe is still an admissible error that can be tolerated in practical implementations burdened by the above-mentioned experimental imperfections. Note that in case of 12 measurement configurations, the ANN misclassifies only 1 in about 400 separable states while simultaneously missclassifying about two times less entangled states then its best performing analytical counterpart, the FEF.

Chapter 3

Entanglement quantification from collective measurements processed by machine learning

Text adopted from *Jan Roik, Karol Bartkiewicz, Antonín Černoch, and Karel Lemr, Physics Letters A, vol. 446, p. 128270, 2022* [A-2].

3.1 Introduction

Quantum entanglement shows immense potential as a resource in various research fields, such as quantum computing [27, 59, 60], quantum cryptography [4] and quantum teleportation experiments [28]. Even though entanglement has been studied for about a century now [22, 23], finding a method for its experimentally feasible quantification for general quantum states is still an open and complex problem [61–64].

The most robust procedure so far seems to be the full quantum state tomography [14, 65], subsequent reconstruction of the density matrix [66], and calculation of entanglement measures. These measures include negativity [15], concurrence, [52, 67] or relative entropy of entanglement [11, 68]. For a review, see Ref. [13]. The problem of full state tomography lies in the unfavorable scaling of the number of measurement configurations as a function of the Hilbert space dimension. Even for a two-qubit system, one needs to apply at least 15 measurement settings while also inevitably obtaining some information on the investigated system that is irrelevant to entanglement quantification. In order to lower the number

of measurement configurations, entanglement witnesses have been proposed [9, 30–49]. However, these instruments are designed to merely detect entanglement and can be used as measures only in limited cases such as quasi-pure states. The concept of nonlinear entanglement witnesses has been introduced [69] as a countermeasure to alleviate the problem of state dependency of entanglement detection. A noteworthy class of nonlinear witnesses is the class of so-called collective witnesses based on simultaneous measurement on multiple instances of the investigated state [43, 45]. Entanglement measures can be estimated from collective measures as well. Analysis reveals that 4 copies of a two-qubit system need to be investigated simultaneously which can prove experimentally too demanding [70]. We limit ourselves to having simultaneously only two copies of the investigated state to overcome this challenge. In this configuration, the relation between the outcomes of a collective measurement and an entanglement measure, say the negativity, is far from trivial.

Machine learning has penetrated many areas of science, helping with finding complex models based on large data sets [71]. Artificial neural networks (ANNs) are particularly well suited for recovering of nonlinear dependencies as they are effective universal function approximators [72]. Not surprisingly thus, ANNs and artificial intelligence, in general, has been used to investigate properties of quantum states, such as entanglement detection [12,50,51], quantification of various properties of quantum states [73–77], or compressed sensing [78, 79]. In this chapter, we use the predictive power of ANNs to estimate quantum state negativity based on the outcomes of collective measurement.

3.2 Collective measurements and data generation

We focus our investigation on quantifying the entanglement of two-qubit states $\hat{\rho}$. The generation of the investigated states and collective measurements were handled similarly, as described in the previous chapter. This investigation aims at efficient entanglement quantification in two-qubit states using as few projections as possible. To achieve this goal, we take inspiration from the concept introduced by Řeháček *et al.* called minimal qubit tomography [14]. The authors established that the minimal set of tomographic projections per one qubit consists of four projections corresponding to states forming a tetrahedral inscribed into a Bloch sphere (see

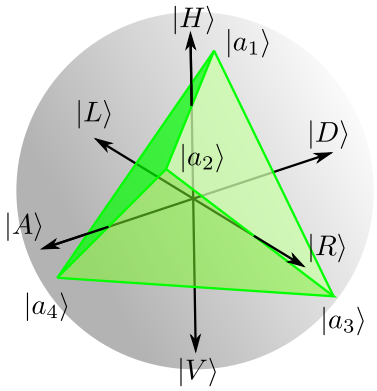

Figure 3.1: Minimal set of tomographic projections visualized on the Poincaré sphere by $|a_j\rangle$ vertices, where $|a_1\rangle = \frac{1}{\sqrt{3}}(1,1,1)$, $|a_2\rangle = \frac{1}{\sqrt{3}}(1,-1,-1)$, $|a_3\rangle = \frac{1}{\sqrt{3}}(-1,1,-1)$, $|a_4\rangle = \frac{1}{\sqrt{3}}(-1,-1,1)$. Black arrows represent $|H\rangle$- horizontal, $|V\rangle$- vertical, $|D\rangle$- diagonal, $|A\rangle$- antidiagonal, $|R\rangle$- circular right-hand, $|L\rangle$- circular left-hand basis states.

Fig. 3.1). One possible set of these projections

$$\begin{aligned}
\hat{\Pi}_1 &= \frac{1}{4}\left(\sigma_0 + \frac{1}{\sqrt{3}}\left(\sigma_x + \sigma_y + \sigma_z\right)\right), \\
\hat{\Pi}_2 &= \frac{1}{4}\left(\sigma_0 + \frac{1}{\sqrt{3}}\left(\sigma_x - \sigma_y - \sigma_z\right)\right), \\
\hat{\Pi}_3 &= \frac{1}{4}\left(\sigma_0 + \frac{1}{\sqrt{3}}\left(-\sigma_x + \sigma_y - \sigma_z\right)\right), \\
\hat{\Pi}_4 &= \frac{1}{4}\left(\sigma_0 + \frac{1}{\sqrt{3}}\left(-\sigma_x - \sigma_y + \sigma_z\right)\right),
\end{aligned} \tag{3.1}$$

is conveniently expressed in terms of Pauli matrices $\sigma_{0,x,y,z}$ [80].

Full two-qubit state tomography still requires at least 15 measurements for this optimal basis, assuming one knows constant state generation rate. A density matrix $\hat{\rho}$ can be estimated from the tomography, and the entanglement quantifier *negativity* is calculated as

$$N_A = 2|\min(\lambda_i)|, \tag{3.2}$$

where $\min(\lambda_i)$ is the smallest eigenvalues of partially transposed density matrix $\hat{\rho}^{PT}$ [15].

For the collective measurement approach to be beneficial, it needs to require at most 7 measurement configurations which is less than one-half of the projections needed for a full state tomography (if we are using two instances simultaneously). Because of the symmetry of $\hat{\rho}_4$, the collective measurement is independent of the swap of local projections, i.e. $P_{xy} = P_{yx}$. Using this fact and considering the minimal basis set $\hat{\Pi}_{1,..,4}$, the maximal independent number of collective measurement configurations is $B = 10$ (see Tab. 3.1). To estimate negativity from a number of configurations $B < 10$, only a subset of the probabilities P_{xy} is selected as indicated in Tab. 3.1. Finding an approximated analytical formulae for quantum states negativity based on a specific number of collective measurement configurations B is a tedious and considerably difficult task. To solve this problem, we turn to the predictive power of artificial neural networks. To this end, uniformly random two-qubit states $\hat{\rho}$ are generated, and the respective probabilities P_{xy} (2.1), as well the analytical value of negativity N_A (3.2), are calculated using the method described above.

3.3 Artificial neural networks

We have programmed the artificial neural networks capable of quantifying the degree of entanglement in terms of negativity for general two-qubit states utilizing the technique of supervised learning. The input dataset is a collection of feature vectors of length B filled with a subset of collective measurement outcomes P_{xy} according to Tab. 3.1. Each vector thus represents B collective measurements carried out on two simultaneous copies of one randomly generated two-qubit quantum state. The output layer (dataset) consists simply of the single value of negativity corresponding to each input vector. The analytical value of negativity N_A is calculated for all randomly generated quantum states from their density matrices (3.2).

The ANN was trained on $4 \cdot 10^6$ feature vectors. A validation dataset of $1 \cdot 10^6$ independent feature vectors was used to implement regularization, and the training was interrupted whenever a stop condition was reached (mean square error on the validation set gets below $1 \cdot 10^{-4}$ and for 10 consecutive epochs does not decrease further). In addition to that, a third independent test set of $1 \cdot 10^6$ feature vectors was used to obtain an unbiased evaluation of the final model. Our ANN struck a balance between complexity and efficiency, allowing us to obtain the best results using two hidden layers with 200 and 150 nodes, respectively as depicted in Fig. 3.2. Decreasing the size of the layers by a factor of two already starts affecting the

model precision, and increasing it by a factor of two does not bring any benefits. Additional layers provide no improvement. The Rectified Linear Unit (ReLU) activation function

$$\mathrm{ReLU}(x) = x^{+} = \max(0, x), \tag{3.3}$$

where x is the input to a neuron, is used between all layers with the exception of the last hidden and the output layer. The output negativity (layer) is calculated using the SoftPlus activation function, a smooth approximation of the ReLU function,

$$\mathrm{SoftPlus}(x) = \ln\left(1 + e^{x}\right). \tag{3.4}$$

Using SoftPlus between the last hidden and output layers outperforms ReLU at this position. We used adaptive moment estimation as an optimizer [81] and mean squared error (MSE) as a loss function

$$\mathrm{MSE} = \frac{1}{n}\sum_{i=1}^{n}(N_A - N_p)^2, \tag{3.5}$$

where n represents the number of all training states, N_A corresponds to analytical values of negativity obtained from the density matrix, and N_p stands for the predicted value of negativity. Experimenting with dropouts did not enhance the learning process.

In summary, the ANNs are used as universal function approximators [72]. Their outputs can be expressed for a three-layer network as

$$f(x, W^{(1)}, W^{(2)}, W^{(3)}) = \phi_3(W^{(3)}\phi_2(W^{(2)}\phi_1(W^{(1)}(x)))), \tag{3.6}$$

where for $n = 1,2,3$ ϕ_n are element-wise nonlinear activation functions acting on the result of matrix multiplication of weight matrices $W^{(n)}$ (the ANN parameters). The activation functions, the number of layers, and the weight matrix dimensions are presented in Fig. 3.2. For a single input sample, x is a vector of B values representing the measurement outcomes given by Eq. (2.1).

We tested the capability of the ANN for various numbers of projections configurations B from 5 to 10, i.e., various lengths of feature vector B. For details on exact measurement configurations used in the case of given feature dimensions B, see Tab 3.1.

As mentioned above, the maximal independent number of collective measurement configurations is $B = 10$. Therefore, we chose this case as our

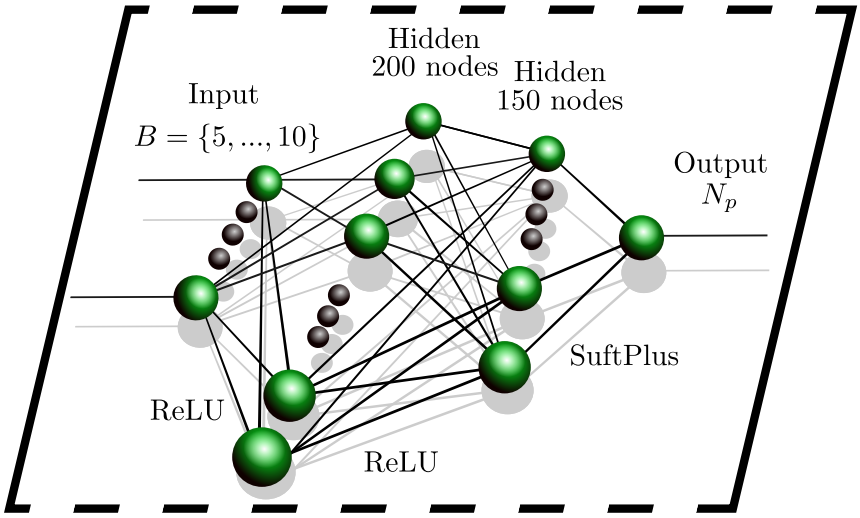

Figure 3.2: Topology of the final ANN model used for negativity N_P prediction from a vector of collective measurements of length B. Two hidden layers are used, containing 200 and 150 nodes, respectively. ReLU and SoftMax are activation functions.

B	Specific projections
5	$\hat{\Pi}_1 \otimes \hat{\Pi}_1, \hat{\Pi}_2 \otimes \hat{\Pi}_2, \hat{\Pi}_3 \otimes \hat{\Pi}_3, \hat{\Pi}_4 \otimes \hat{\Pi}_4, \hat{\Pi}_1 \otimes \hat{\Pi}_3$
6	$B = 5, \wedge \hat{\Pi}_2 \otimes \hat{\Pi}_4$
7	$B = 6, \wedge \hat{\Pi}_1 \otimes \hat{\Pi}_4$
8	$B = 7, \wedge \hat{\Pi}_1 \otimes \hat{\Pi}_2$
9	$B = 8, \wedge \hat{\Pi}_2 \otimes \hat{\Pi}_3$
10	$B = 9, \wedge \hat{\Pi}_3 \otimes \hat{\Pi}_4$

Table 3.1: List of specific projection settings P_{xy} for a given number of measurements B. Note that B is consecutively the length of input feature vectors in the ANNs.

starting and reference point. From there, we gradually reduced the number of provided projections down to $B = 5$. The most impactful results are obtained for $B = 7$ because, at that point, the number of projections drops below one-half of the projections needed for a full state tomography making this setting our primary success indicator. We used the coefficient of determination R^2

$$R^2 = 1 - \frac{SS_{res}}{SS_{tot}}, \tag{3.7}$$

and standard deviation

$$\tau = \frac{1}{\sqrt{n}} \sqrt{\sum_{i=1}^{n} ((N_A - N_p) - \mu)^2}, \tag{3.8}$$

to quantify the capabilities of the ANNs. Where the total sum of squares SS_{tot} and residual sum of squares SS_{res} are defined as

$$\begin{aligned} SS_{tot} &= \sum_i (N_A - \bar{N})^2, \\ SS_{res} &= \sum_i (N_A - N_p)^2, \\ \bar{N} &= \frac{1}{n} \sum_{i=1}^{n} N_A, \end{aligned} \tag{3.9}$$

$\bar{N}$ represents the mean value of analytically calculated negativity, and the mean average is obtained as

$$\mu = \frac{1}{n} \sum_{i=1}^{n} (N_A - N_p). \tag{3.10}$$

3.4 Results.

First, we provided the ANN with all available information about the investigated state (i.e., $B = 10$ projections) to set the benchmark. In this specific case, the ANN was able to reach $R^2 = 0.996$ and $\tau = 0.01$ (see Fig. 3.3). For $B = 10$, network model gives our best approximation of the negativity function $N(\hat{\rho})$ using only two copies of the investigated state and collective measurements. In the next step, we reduced the number of projections to $B = 9$. As expected, the performance of the network decreased to $R^2 = 0.993$ and $\tau = 0.02$. Further decrease in the number of projections to $B = 8$ did not reveal anything noteworthy but merely confirmed the trend established

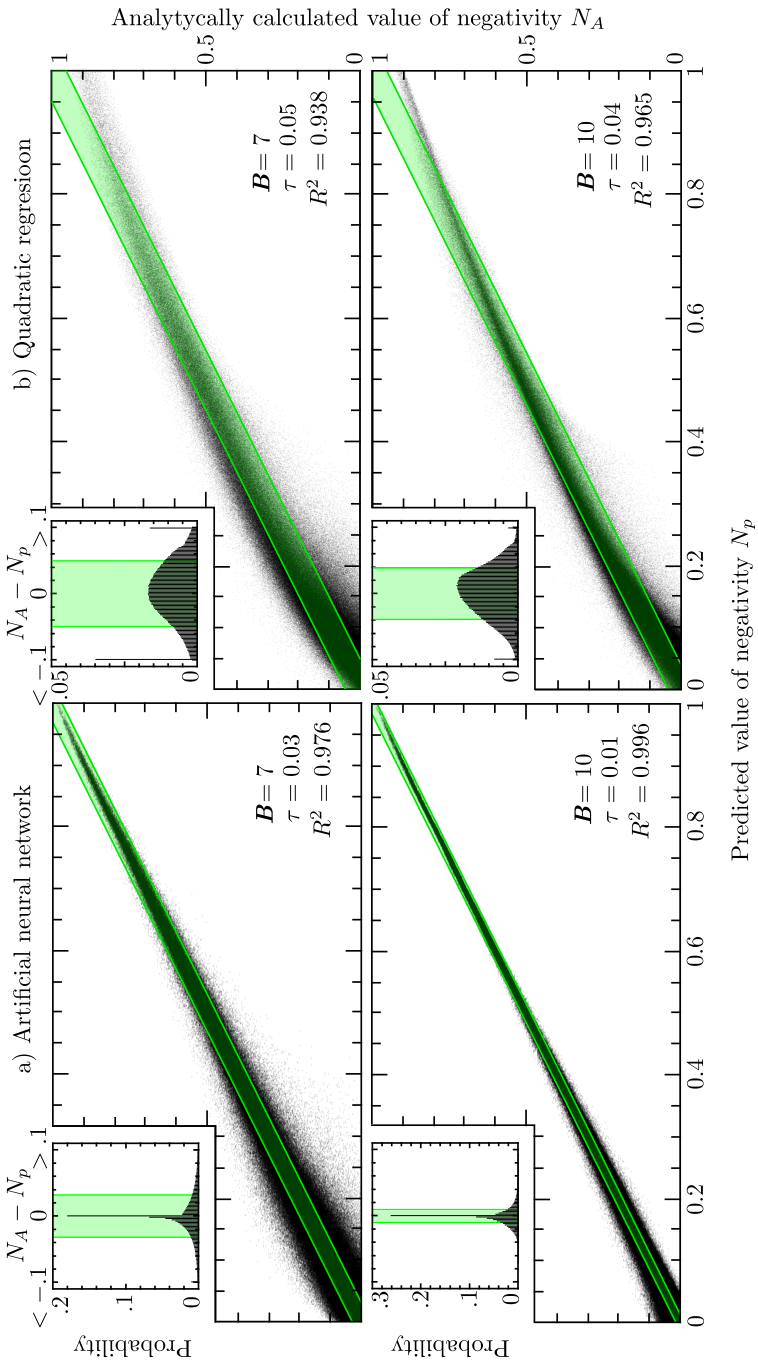

Figure 3.3: Comparison between analytically calculated negativity N_A and negativity predicted N_p by (a) artificial neural network and (b) quadratic regression for $B = 10$ and 7 configurations, respectively. In addition, the graphs include insets depicting histograms of the difference between N_A and N_p. Every tiny black dot corresponds to one of $1 \cdot 10^6$ tested random states. The coefficient of determination R^2 and standard deviation τ are also included in the legend. In an ideal case, all dots should lie on a diagonal line $N_A = N_p$. Green stripes depict standard deviation $\pm\tau$ from such an ideal case.

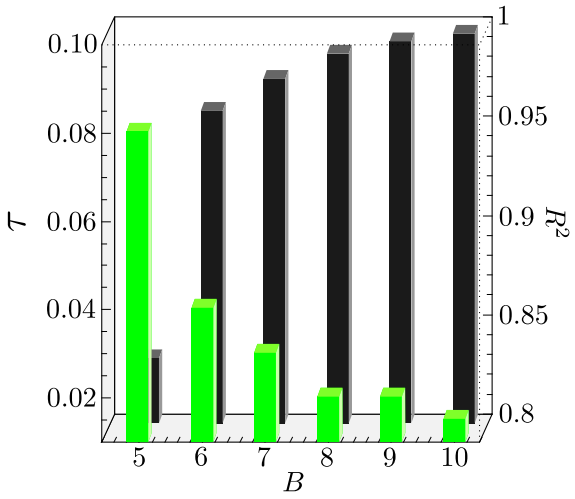

Figure 3.4: The coefficient of determination R^2 (represented by black back columns) and standard deviation τ (represented by green front columns) are plotted for all measurement configurations B to visualize trends in the results.

above. The performance of the ANN taught on $B = 7$ projections represents the most notable result $R^2 = 0.976$ and $\tau = 0.03$ (see Fig. 3.3 for $B = 7, 10$ and Fig. 3.5 for other values of B) because, at this point, we reduced the number of projections under the full tomography requirements. Obtained results are similar to the limits of the analytical calculations performed on the estimated density matrix from actual experimental tomography data. Those calculations cannot be completely accurate due to unavoidable measurement uncertainties, which usually contribute to final analytical errors by a similar margin, i.e., $\tau = 0.03$ [82]. When the number of projections dropped to $B = 6$ we noticed some decline in the prediction capabilities ($R^2 = 0.961$ and $\tau = 0.04$). Even for $B = 6$ measurement configurations, the observed prediction error is still quite comparable to experimental full state tomography. We tried to limit the number of projections as much as possible, but we drew the line at $B = 5$. In this case, the ANN performance pecked at $R^2 = 0.841$ and $\tau = 0.08$. At this point, the prediction error is already significant, and therefore we did not proceed with further decreasing of B. For an overview of the results, see Fig. 3.4.

In Fig. 3.3, we have also compared the ANN models to quadratic regression models for $B = 7, 10$. The ANNs use significantly more model pa-

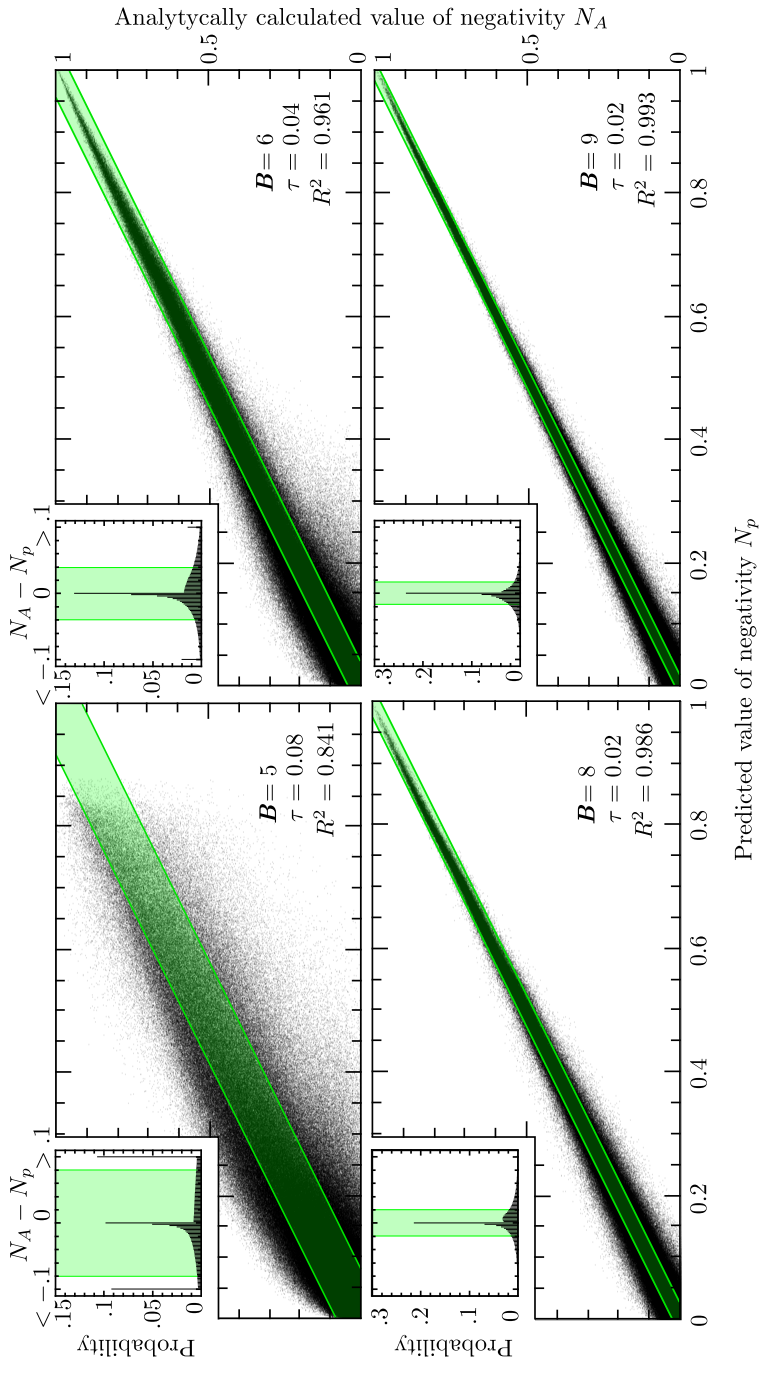

Figure 3.5: Comparison between analytically calculated negativity N_A and negativity predicted N_p by artificial neural network for $B = 5,6,8$ and 9 configurations respectively. In addition, the graphs include insets depicting histograms of the difference between N_A and N_p. Every tiny black dot corresponds to one of $1 \cdot 10^6$ tested random states. The coefficient of determination R^2 and standard deviation τ are also included in the legend. In an ideal case, all dots should lie on a diagonal line $N_A = N_p$. Green stripes depict standard deviation $\pm\tau$ from such an ideal case.

rameters than our regression models, but they perform much better. The coefficient of determination for the ANN models is typically larger by 0.03 if compared with the quadratic models. The typical root mean square difference between the predicted values N_p of the ANNs and quadratic regression models is circa 0.17, and it does not depend strongly on the number of measurement configurations B. However, there is an actual benefit of using the quadratic regression models because by doing so, we are able to directly obtain reasonably compact approximate analytical formulae for negativity as functions of assorted collective measurements. Note that regression models up to the fifth order were also tested and did not outperform the ANNs.

3.5 Conclusions

The above-presented results demonstrate a significant potential of ANNs together with collective measurements for entanglement quantification. Even for $B = 6$ and 7 measurement configurations, the collective measurement performs similarly to experimental full quantum state tomography committing the predictive error of about 3% (in terms of standard deviation). Considering that the particular geometry of collective measurement also overlaps with the entanglement swapping setup [83], implementing entanglement quantification using this configuration can prove interesting for future quantum communication networks [84]. The method presented in this chapter can be used for effective entanglement quantification in entanglement swapping-based communication networks. Moreover, our previous research on the binary classification of entangled/ separable states indicates that the ANN trained on numerically generated quantum states also performs especially well on noisy experimental data [A-1] (at least on limited classes of quantum states). While nonlinear models are expected to function poorly on noisy data, they could perform reasonably well on data burdened with typical experimental error [70]. Although this work investigates the quantification of entanglement that is more demanding than comparison to simpler binary classification, we feel encouraged to conclude that the trained ANNs may also perform adequately on experimental data. However, the development of corresponding experimental setup implementing the set of projectors (3.1) and gathering a sufficient amount of real quantum state data goes well beyond the scope of this investigation. The ANNs were implemented using the TensorFlow 2.0 [57] and Keras [85] libraries.

Chapter 4

Routing in quantum communications networks using reinforcement machine learning

Text adopted from *Jan Roik, Karol Bartkiewicz, Antonín Černoch, and Karel Lemr, submitted (2023)* [A-3].

4.1 Introduction

Efficient communication has played a crucial role in the evolution of all civilizations since antiquity [86, 87]. As the evolution continued, our society began to globalize, and so have our communications needs, ultimately leading to the introduction of the Internet [88]. Nowadays, even these classical communications networks seem outdated, facing the development in the field of quantum communications [89]. The first proposed quantum communications protocols were designed for a one-to-one quantum key distribution (QKD) [90–92]. Subsequent strategies to encompass more parties have been proposed [92, 93]. One promising approach is the so-called teleportation-based quantum networks facilitated by standard or controlled teleportation [94,95]. The idea is to concatenate many teleportation-based cells into a large global network, i.e., the quantum Internet [96]. Many studies have discussed this concept's potential [97–99], the network's pos-

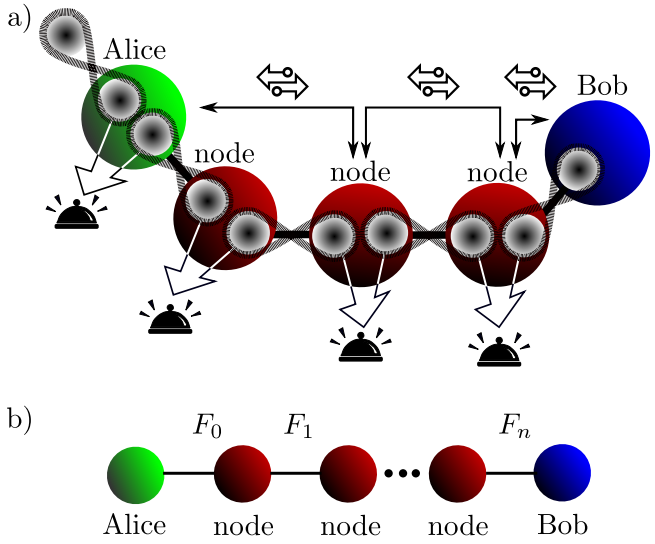

Figure 4.1: Schemes represent entanglement swapping from the initial to the final point in the quantum communications network. a) Each node possesses pair of particles belonging to two different entanglement states symbolized by the two black balls inside the nodes, black line between nodes depicts a quantum channel, green node symbolizes the initial point "Alice", red balls depict intermediate nodes used for entanglement swapping, and blue ball represents the final point "Bob". Bell icon mark where Bell measurement takes place and swap icon highlight where entanglement swapping is carried out. b) Characterization of the road between the initial and final point where $F_0, \ldots, F_n$ are singlet fractions shared by two neighboring nodes.

sible topologies [100], platforms to realize it on [101], and fundamental problems to overcome [16].

Quantum networks, however, aim beyond mere QKD, which we must consider when designing quantum networks. The major problem that needs to be addressed is finding an efficient method for optimal dynamic routing in these large-scale quantum networks. It seems that teleportation (entanglement swapping) is, for now, the best method for establishing connections between distant parties in quantum networks [102]. Also, note that entanglement swapping is the core ingredient for quantum repeaters [103] and relays [104], allowing combating unfavorable scaling of losses.

The unique features of quantum information prevent reliably employing classical tools such as shortest path and tree search algorithms [105]. This investigation provides solutions to the routing problem in teleportation-based networks using reinforcement machine learning. The connection between two distant parties (Alice and Bob) in these networks is established by repeated use of entanglement swapping by several intermediate nodes resulting in an entangled state $\hat{\phi}$ shared by the abovementioned parties, Alice and Bob (see Fig. 4.1) [83]. Once they share an entangled state, Alice and Bob are free to use it for secret key sharing [4], quantum state teleportation [6] or dense coding [106]. There are many possibilities to quantify the quality of the repeated entanglement swapping and the quality of the shared entangled state between Alice and Bob [13, 25]. We chose the singlet fraction F as the figure of merit because for bipartite entangled states, F can be directly used to evaluate the usefulness of $\hat{\phi}$ for quantum teleportation [107]. Singlet fraction

$$F(\hat{\phi}) = \max_{|\psi\rangle} \langle\psi|\hat{\phi}|\psi\rangle, \tag{4.1}$$

is defined as the maximal overlap of the investigated state $\hat{\phi}$ with any maximally entangled state $|\psi\rangle$. Maximal achievable teleportation fidelity f of a qubit state is then calculated as

$$f = \frac{2F+1}{3}. \tag{4.2}$$

One can naively think that the singlet fraction of the final state shared by Alice to Bob F_{AB} is obtained as a product of singlet fractions of the entangled states introduced in the repeated n entanglement swappings (see Fig. 4.1)

$$F_{AB} = \prod_{i=0}^{n} F_i, \tag{4.3}$$

alternatively, one can establish an effective *distance d* between Alice and Bob using a logarithm of the singlet fraction

$$d = -\log F_{AB} = -\sum_i \log F_i. \tag{4.4}$$

However, this is not generally true. For example, in cases of amplitude damping [18] or correlated phase noise [19], errors can cancel each other out. If Eq. (3) and Eg. (4) were to hold, one should be able to assign a single quantifier to each quantum channel between nodes and use any graph

path or tree-finding algorithm such as the Dijkstra algorithm and find the route minimizing the distance d [108]. As we show later in this chapter, this yields suboptimal solutions. Note that even prominent dynamic algorithms such as Bellman-Ford [109] and A* [110] cannot handle these types of errors.

One possible solution capable of handling quantum effects is a brute force in the form of the Monte Carlo algorithm. The only downside is Monte Carlo's exponential scaling with the number of nodes. Such a scaling becomes a game stopper, especially in the case of an evolving network where it needs to be repeatedly executed. Hence, a smarter strategy needs to be adopted. In this chapter, we propose using the proximal policy optimization (PPO), an artificial intelligence-based algorithm developed to solve complex evolving problems [20]. This algorithm is commonly used in the gaming industry, where we found inspiration for how to approach the routing problem. We designed our network as a map in a game for the agent to play, intending to find the optimal path through the quantum network. We compare the performance of the PPO against the Monte Carlo and the Dijkstra algorithm demonstrating PPO's virtues.

4.2 Quantum network topology

We found the inspiration for our network topology in the low-density parity-check code structure, one of the possible topologies considered for designing the 6G networks. For the details on the topology, see Fig. 4.2 [21]. This network simulates a real-world scenario where several local users form groups connected among themselves by central nodes. We chose this particular topology mainly due to its robustness against local connection problems, contributing to steady performance. In case of random malfunction in any specific node, this topology offers several possible reroutes to ensure stability. Each connection in the network structure represents a quantum channel using which two neighboring nodes share an entangled two qubit state. For simplicity, we limit the network topology to a maximum of 4 connections per node. Moreover, each node can perform entanglement swapping, i.e., Bell measurement. All shared entangled states are fully characterized by their density matrices. This representation allows us to fully describe how noisy or damaged each connection is. We can easily simulate different sources of disturbance, such as white noise in the channel or amplitude damping. These essential characteristics enable us to simulate various scenarios in the communications network that we later

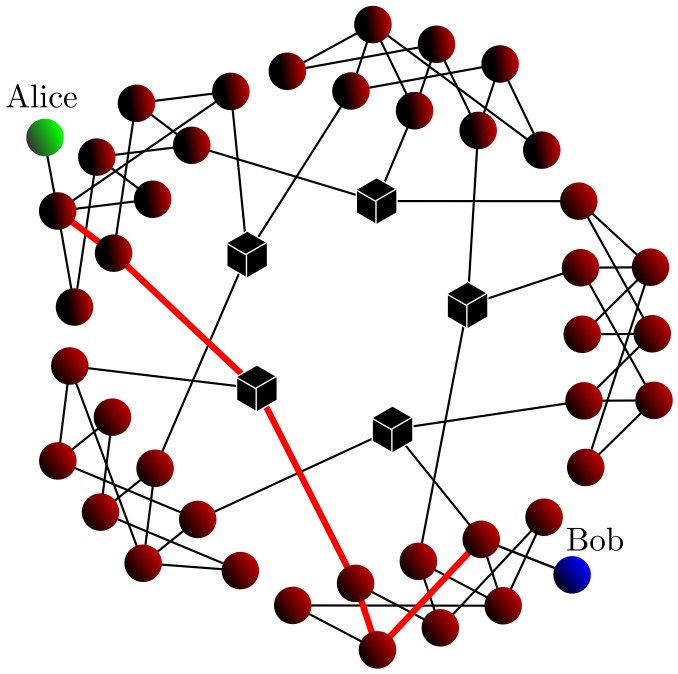

Figure 4.2: This figure shows a visualization of the quantum communications network. The entangled photon pair marked “Alice” represents the initial position for our agents, and blue circle named “Bob” marks the ending point of the route. Full black lines set possible routes for entanglement swapping, red thick lines highlight the optimal solution under ideal conditions, and black cubes represent primary connection nodes between local clusters.

present in the Results section.

The ultimate goal is to distribute entangled state between Alice and Bob. As mentioned in the previous section, the quality of this state is given in terms of singlet fraction F_{AB}, which we maximize. We cast this task as a “game” for the tested algorithms to play. The final reward is received in proportion to F_{AB}. Every connection can be used in each game only once because the used entangled pair is consumed in entanglement swapping. We choose the initial and final users’ positions so that the agent can successfully connect them in a given number of actions. We made the routing in the network realistic by ensuring that even the unperturbed connections have a singlet fraction of the distributed state $F = 0.99$ by adding a

corresponding amount of white noise, forcing the PPO algorithm towards the shortest path solutions. To represent white noise, we model the shared entangled states in the form of Werner states

$$\hat{\rho}_w = p|\psi^-\rangle\langle\psi^-| + (1-p)\hat{1}/4. \tag{4.5}$$

$|\psi^-\rangle = (|01\rangle - |10\rangle)/\sqrt{2}$ represents singlet Bell state, $\hat{1}/4$ stands for the maximally mixed state, and p is the mixing parameter. Amplitude damping, on the other hand, is represented by generalizing the Bell states $|\psi^-\rangle$ to

$$|\psi_g^-(\theta)\rangle = \cos(\theta)|01\rangle - \sin(\theta)|10\rangle, \tag{4.6}$$

where $\theta \in [0; \frac{\pi}{2}]$ is the damping parameter. Lastly, an arbitrary phase shift can be described as

$$|\psi_s^-(\phi)\rangle = (|01\rangle - e^{i\phi}|10\rangle)/\sqrt{2}, \tag{4.7}$$

where $\phi \in [0; \pi]$ is the phase shift parameter and if uncompensated and random, renders the state shared between Alice and Bob effectively mixed.

4.3 Routing algorithms

We tested different algorithms capable to solve routing in quantum networks and compared their performance. Namely, we tested the PPO, Dijkstra algorithm, and Monte Carlo method on the quantum communications network. PPO is a policy gradient method for reinforcement learning which uses multiple epochs of stochastic gradient ascent to perform each policy update. It is well known for the simplicity of implementation to various problems and overall performance compared to similar family algorithms. We use stable baseline 3 framework [111] and its implementation of the PPO in our work.

The PPO agents starts at Alice's node. It can choose from at most four actions corresponding to the maximum number of connections any node can have. If the agent chooses an invalid action (i.e., a non-existing connection), the game ends with a negative reward. If a valid link is selected, the agent moves to the node connected by the chosen connection (action). At this point, entanglement swapping is implemented, leading to a shared entangled state between Alice and the connected node. Selecting action and implementing entanglement swapping constitutes one action. A maximum of 15 actions limits the agent; if depleted, the game ends. The preliminary reward is calculated at the end of each action using the formula

$$R_p = F_{A_i} - F_{A_{i-1}}. \tag{4.8}$$

where F_{A_i} stands for the singlet fraction of the newly established entangled state while $F_{A_{i-1}}$ is the singlet fraction resulting from entanglement swapping in the preceding action ($F_{A_0} = 1$ in case of the first action). We tuned the n-steps hyperparameter of the PPO according to the complexity of the designed quantum network topology. Note that the n-steps hyperparameter determines the number of actions the agent takes before updating the parameters of its policy. We kept all other hyperparameters in default values because we did not notice significant changes when tuning them. It is the reward function structure that has the most noticeable influence on the agent's performance. We save the PPO's policy after every 100–5000 games based on the scenarios' complexity. If the agent reaches the final destination (Bob), it receives a final reward

$$R = 100F_{AB}. \tag{4.9}$$

In case of the Monte Carlo algorithm, we applied the same game rules as for the PPO. So, we can obtain a straightforward comparison. The only difference is that Monte Carlo chooses its actions randomly in each game with no intelligent policy.

Dijkstra's algorithm, on the other hand, needs more information and the data structure of the task. Unlike the previous agents, it needs to know the exact topology of the communications network ahead as well as information about each connection. Therefore, the Dijkstra algorithm does not operate under the same conditions as the previously mentioned agents. At the expense of requiring all the information, it is very efficient at finding distance d from Alice to Bob.

4.4 Results

Firstly, we investigate routing in a quantum network burdened solely by white noise. This scenario is close to the classical network because white noise is additive and can not be compensated. In a quantum network, however, other types of errors can occur. As examples of such errors, we consider amplitude damping and correlated phase noise which we investigate in the second and third subsections. Finally, a dynamically evolving network noise is considered in the last subsection.

Intermediary nodes (count)	6	8	10	12	14	16
			Number of iterations			
PPO	780	1280	6880	7680	11840	41K
Monte Carlo	644	4310	95K	250K	4M	200M
Dijkstra				1012		

Table 4.1: Results of the three agents applied to the networks of different complexity. This complexity is parametrized by the minimal number of intermediary nodes (first row of the table) that need to be visited in order to find a valid routing solution. The number of iterations is the average number of iterations required to find a solution for a particular topology. Here M = 10^6 and K = 10^3.

4.4.1 Network affected by white noise

We start with a completely operational network. A singlet fraction $F = 0.99$ characterizes all connections. Optimal routing through this network between Alice and Bob involves 6 intermediary nodes. Then we started introduce damaged connections (i.e., connections with $F = 0.6$), thus increasing the number of the intermediary nodes (8,10,12,14,16) required for finding the optimal solution. The performances of the three agents (PPO, Monte-Carlo, Dijkstra) are summarized in Tab. 4.1.

The Monte Carlo method offers comparable performance to PPO only in the case of the simplest scenario (fully operational network with 6 intermediary nodes to find a solution). The more complex the scenario is, the more prominent the PPO's performance gain becomes. More specifically, in the case of a network where at least 16 intermediary nodes are required to find a solution, PPO outperforms the Monte Carlo method by a factor of about 5000. For visualization see Fig. 4.3. Given the additivity of white noise, the Dijkstra algorithm significantly outperforms the PPO and Monte Carlo in these almost classical scenarios. However, the situation changes with the introduction of purely quantum noise.

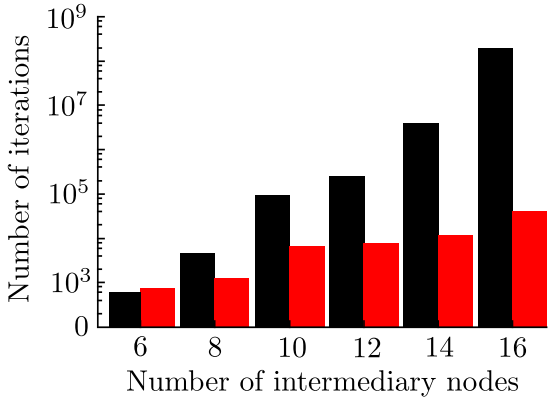

Figure 4.3: The graph compares the performance of the PPO algorithm, represented by the red (right) columns, and the Monte Carlo algorithm, depicted by black (left) columns, on different scenarios requiring a given number of passes through intermediary nodes in the quantum networks.

4.4.2 Network affected by amplitude damping

Amplitude damping, as introduced in Eq. 4.6, skews the amplitude balance towards one of the two components ($|01\rangle$ or $|10\rangle$). As a result, the singlet fraction decreases. Two connections with mutual opposite component damping can rebalance the amplitudes increasing the singlet fraction (at the expense of overall losses). This feature is intractable by greedy or dynamic algorithms such as Dijkstra, Bellman-Ford, or A*. In order to use those algorithms, one needs to save all preliminary solutions and compare them, which would cause exponential scaling of the algorithm complexity. Ultimately, the agent needs to figure out that in order to complete the task, it needs to find such a route where individual amplitude damping cancel each other out as much as possible. We forced the agent to use this strategy by designing scenarios where the agent must choose at least one amplitude-damped connection to reach the final destination. Moreover, the resulting singlet fraction is maximized when a second (opposite) amplitude-damped connection is chosen by the agent. Similar to the previous subsection, we present the agent with scenarios ranging from 6–16 intermediary nodes.

The agents' performance is summarized in Tab. 4.2 and plotted in Fig. 4.4. One can notice that due to these complex initial conditions, the Monte Carlo algorithm performs slightly better than PPO when the optimal path

Intermediary nodes (count)	6	8	10	12	14	16
	Number of iterations					
PPO	1740	13K	14K	15K	54K	60K
Monte Carlo	1K	14K	94K	2M	5M	200M

Table 4.2: Results of the two agents applied to the networks of different complexity, including effects such as amplitude damping. This complexity is parametrized by the minimal number of intermediary nodes (first row of the table) that need to be visited in order to find a valid routing solution. The number of iterations is the average number of iterations required to find a solution for a particular topology. Here M = 10^6 and K = 10^3.

consists of 6 intermediary nodes. Both methods show similar performance for the 8 intermediary nodes solution; as of 10 intermediary nodes solution onward, the PPO significantly outperforms the Monte-Carlo. In the most complex scenario, i.e. 16 intermediary nodes, the PPO outperforms the Monte Carlo method by a factor of about 3300.

4.4.3 Network affected by correlated phase noise

This subsection demonstrates how agents handle another type of reversible damage caused by the correlated phase noise. These scenarios are motivated by one of the practical approaches towards quantum information distribution proposed by Xu *et al.* [19]. Testing Dijkstra algorithms is again pointless for the reasons we mentioned in the previous subsection. To demonstrate the versatility of the PPO agent, a brand new set of scenarios involving 6-16 intermediary nodes were generated. In the current scenario, the agent starts from the initial node Alice and in the first action, it can only choose from paths damaged by the correlated phase noise. The agent aims to search the network for a suitable path to reverse the initial correlated phase shift. If successful, it must then find the final node, Bob.

Results of this test are shown in Tab. 4.3 and plotted in Fig. 4.5. One can notice that in the case of the 6 intermediary nodes scenario, the Monte Carlo slightly outperforms the PPO algorithm. However, the PPO agent

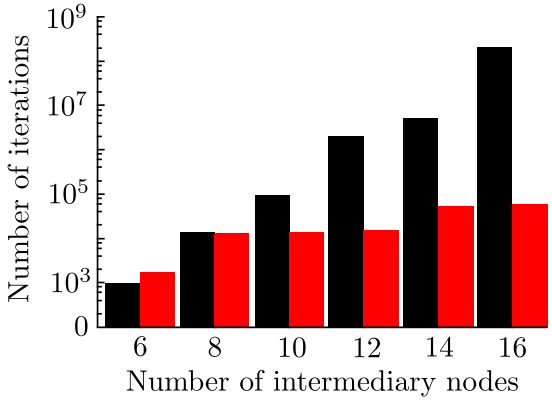

Figure 4.4: The graph compares the performance of the PPO algorithm, represented by the red (right) columns, and the Monte Carlo algorithm, depicted by black (left) columns, on different scenarios in the quantum networks where we also introduced connections affected by amplitude damping.

performs significantly better for all more complex scenarios from 8 intermediary nodes onward.

4.4.4 Evolving quantum network

Ultimately, we test the agents on dynamically evolving scenarios in our quantum network. The agents' goal in this final test is to maximize the overall functionality of the network throughout the evolutions. These scenarios reflect the realistic behavior of real-world quantum networks where various errors appear at random places and times. The entire routing task lasts for 10^6 iterations, during which the quantum network undergoes ten scenarios (i.e., ten events when various connections become damaged or unperturbed). The evolution continues regardless of the agent's success. In this final test, we use all three types of errors discussed in previous chapters, namely white noise, amplitude dumping, and correlated phase noise. To make the interpretation of the results clear, we set some ground rules. Suppose the agent finds a solution (i.e., a path between Alice and Bob with $F > 0.8$) to the current scenario. In that case, it will use this solution for as long as its singlet fraction remains $F > 0.8$ (i.e., until the scenario evolves). PPO agent at that point also saves its current policy. After the situation

Intermediary nodes (count)	6	8	10	12	14	16
	Number of iterations					
PPO	1320	2700	10K	20K	27K	39K
Monte Carlo	780	4672	45K	500K	4M	22M

Table 4.3: Results of the two agents applied to the networks of different complexity, including effects such as correlated phase noise. This complexity is parametrized by the minimal number of intermediary nodes (first row of the table) that need to be visited in order to find a valid routing solution. The number of iterations is the average number of iterations required to find a solution for a particular topology. Here M = 10^6 and K = 10^3.

evolves, both agents search for a new solution. PPO starts searching from the last saved policy and Monte Carlo randomly from scratch. Each evolution introduces errors so that the previous solution is no longer valid ($F < 0.8$). Hence agents need to find a new route. This condition does not mimic the natural network behavior, but it is the most extreme case where the PPO agent faces the most disadvantageous conditions. Resulting success rates are shown in Fig. 4.6. From the obtained results, it is clear that if we let agents deal with an undamaged or slightly damaged network (scenarios 1,2,10), both agents can keep the network functional for more than 95% of the time. If the scenario becomes a bit more complex (scenario 6), the PPO agent slightly outperforms the Monte Carlo agent. For even more complex scenarios, Monte Carlo could not find a solution in a given amount of iterations. Due to these poor results, Monte Carlo kept the network functional for 37.5% of the overall time. On the other hand, the PPO found a solution in 10/10 scenarios and kept the network functional for 93.4% of the overall time.

4.5 Conclusions

This investigation compares three different algorithms (PPO, Djikstra, and Monte Carlo) for route-finding in quantum communications networks. We

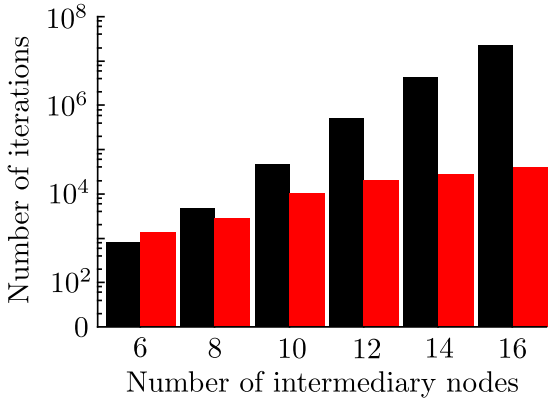

Figure 4.5: The graph compares the performance of the PPO algorithm, represented by the red (right) columns, and the Monte Carlo algorithm, depicted by black (left) columns, on different scenarios, staged in the quantum networks where we also introduced connections causing correlated phase noise.

benchmark these algorithms on various scenarios in a realistic network topology using singlet fraction as the figure of merit. In these scenarios, we introduce additive white noise as well as purely quantum errors such as amplitude damping and correlated phase noise.

We explicitly show that the non-additivity of quantum errors prevents traditional graph path or tree-finding algorithms (Djikstra) from finding the optimal solution. While the Monte Carlo search allows finding such optimal solutions, its exponential scaling makes its deployment prohibitive in large complex networks. We demonstrate that reinforcement machine learning in the form of the PPO algorithm circumvents the limitations of both aforementioned approaches. It can cope with purely quantum errors and, simultaneously, does not suffer from unfavorable scaling.

Our numerical model reveals that the PPO advantage over mere Monte-Carlo search becomes significant when the number of intermediary nodes in the path increases (e.g., for 16 intermediary nodes, PPO outperforms Monte-Carlo by a factor of several thousand). Moreover, in a dynamically evolving quantum network, the PPO could maintain an operational route for about 93% of the time, while Monte Carlo for less than 38%. We believe that our research further promotes reinforcement learning as an invaluable method for improving quantum communications.

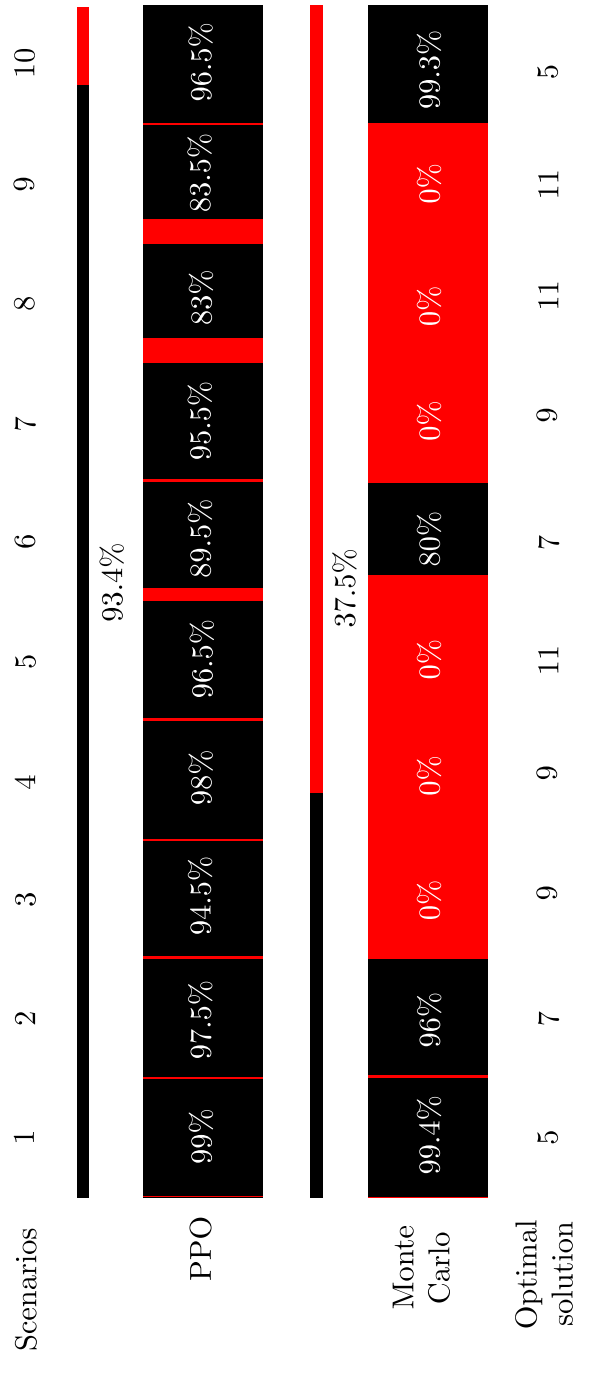

Figure 4.6: Illustration of the Agents' performance on the evolving quantum communication network. Thin stripes show the overall functionality of the quantum network throughout its evolution, and the thick stripes show the functionality during each scenario of its evolution.

Chapter 5

Conclusions

"*The saddest aspect of life right now is that science gathers knowledge faster than society gathers wisdom.*"

-Isaac Asimov

Humankind stands on the verge of a new era, "The golden age" of artificial intelligence. Tasks that were just a few years ago mentioned only in the context of sci-fi literature are nowadays becoming reality. Despite all recent breakthroughs, there still lies a long road ahead to unveil the full potential of artificial intelligence. Based on the achieved results, artificial intelligence has already earned its place as a valuable tool in research. The author firmly believes that artificial intelligence has the potential to shed some light on the fundamental problems of science. Further deployment of artificial intelligence into fields such as quantum data processing may significantly speed up the development of essential technologies, such as large-scale quantum networks.

This thesis presented two fundamental problems of quantum physics and one of quantum data processing. The first problem focused on optimizing the detection of quantum states. The promising results in detecting entangled states motivated follow-up research focused on quantifying the amount of entanglement. The third research task was dedicated to the problem of finding the optimal route in quantum networks. In all three cases, the presented tasks have quantum nature, and to find the solution, we deployed artificial intelligence. That is why Chapter 2 briefly introduces the method and terminology of artificial intelligence and machine learning, and the second half of Chapter 2 establishes basic terms of

quantum data processing.

Chapter 3 highlights the potential of artificial neural networks to binary classify random two-qubit states as entangled or separable. Achieved results demonstrate that given the same amount of resources (i.e., the number of unique collective measurements), ANN surpassed all tested analytical entanglement witnesses. Furthermore, we showed that ANN trained on artificially generated data could be applied to actual experimental data with similar success.

In Chapter 4, we discussed the generalization of the idea from Chapter 3. Here we present the potential of the ANN not just to classify general two-qubit states but also the capability to quantify their amount of entanglement. The ANN aimed to match the negativity values obtained from the full-state tomography. We showed that, given fewer resources, ANN could still maintain comparable prediction capabilities as full-state tomography. Furthermore, we demonstrated that ANN performs favorably in comparison with polynomial regression.

In the fifth chapter, we moved from the fundamental problems of quantum physics to obstacles restricting progress in applied research. Here we tested three conceptually different approaches toward route finding in quantum networks. According to our results, the classical route-finding algorithms struggle to find an optimal solution due to the presence of quantum errors. On the other hand, the proximal policy optimization demonstrated the ability to solve even complex scenarios involving different types of errors while maintaining favorable scaling. During the ultimate test on the evolving quantum network, PPO dominated the Monte Carlo algorithm and decisively proved its potential.

As a closing thought, the author wants to declare that the presented results have already caught the attention of the broader scientific community. Based on the results presented in Chapter 4, we established an international collaboration focused on the follow-up research with a promise to unveil some fundamental dependencies of entanglement detection. We also plan to build an experimental setup capable of doing collective measurements in the minimal set of tomographic projections to test the ANN quantification of entangled states on a real-experimental dataset.

Author's publications

[A-1] J. Roik, K. Bartkiewicz, A. Černoch, and K. Lemr, "Accuracy of entanglement detection via artificial neural networks and human-designed entanglement witnesses," *Physical Review Applied*, vol. 15, no. 5, p. 054006, 2021.

[A-2] J. Roik, K. Bartkiewicz, A. Černoch, and K. Lemr, "Entanglement quantification from collective measurements processed by machine learning," *Physics Letters A*, vol. 446, p. 128270, 2022.

[A-3] J. Roik, K. Bartkiewicz, A. Černoch, and K. Lemr, "Routing in quantum communications networks using reinforcement machine learning", submitted (2023).

[A-4] J. Roik, K. Lemr, A. Černoch, and J. Soubusta, "Calibration of commercially available RGB colorimeters using a spectrometer," *Jemná mechanika a optika*, vol. 67, p. 24, 2022.

[A-5] J. Roik, K. Lemr, and A. Černoch, "Testování a kalibrace RGB kalorimetrů," *Jemná mechanika a optika*, vol. 63, p. 170, 2018.

[A-6] J. Roik, K. Lemr, A. Černoch, and K. Bartkiewicz, "Interplay between strong and weak measurement: comparison of three experimental approaches to weak value estimation," *Journal of Optics*, vol. 22, no. 6, p. 065202, 2020.

[A-7] K. Bartkiewicz, P. Tulewicz, J. Roik, and K. Lemr, "Collaborative generative quantum machine learning on a quantum computer," arXiv preprint arXiv:2112.13255, 2021.

Bibliography

[1] K. Lemr, K. Bartkiewicz, A. Černoch, and J. Soubusta, "Resource-efficient linear-optical quantum router," *Physical Review A*, vol. 87, no. 6, p. 062333, 2013.

[2] E. Meyer-Scott, M. Bula, K. Bartkiewicz, A. Černoch, J. Soubusta, T. Jennewein, and K. Lemr, "Entanglement-based linear-optical qubit amplifier," *Physical Review A*, vol. 88, no. 1, p. 012327, 2013.

[3] J. Jašek, K. Jiráková, K. Bartkiewicz, A. Černoch, T. Fürst, and K. Lemr, "Experimental hybrid quantum-classical reinforcement learning by boson sampling: how to train a quantum cloner," *Optics express*, vol. 27, no. 22, pp. 32454–32464, 2019.

[4] N. Gisin, G. Ribordy, W. Tittel, and H. Zbinden, "Quantum cryptography," *Rev. Mod. Phys.*, vol. 74, pp. 145–195, Mar 2002.

[5] A. Harrow, P. Hayden, and D. Leung, "Superdense coding of quantum states," *Physical review letters*, vol. 92, no. 18, p. 187901, 2004.

[6] S. Pirandola, J. Eisert, C. Weedbrook, A. Furusawa, and S. L. Braunstein, "Advances in quantum teleportation," *Nature photonics*, vol. 9, no. 10, pp. 641–652, 2015.

[7] D. P. DiVincenzo, "Quantum computation," *Science*, vol. 270, no. 5234, pp. 255–261, 1995.

[8] Ł. Rudnicki, P. Horodecki, and K. Życzkowski, "Collective uncertainty entanglement test," *Physical Review Letters*, vol. 107, no. 15, p. 150502, 2011.

[9] J. F. Clauser, M. A. Horne, A. Shimony, and R. A. Holt, "Proposed experiment to test local hidden-variable theories," *Phys. Rev. Lett.*, vol. 23, pp. 880–884, Oct 1969.

[10] K. Bartkiewicz, P. Horodecki, K. Lemr, A. Miranowicz, and K. Życzkowski, "Method for universal detection of two-photon polarization entanglement," *Phys. Rev. A*, vol. 91, p. 032315, Mar 2015.

[11] V. Vedral and M. B. Plenio, "Entanglement measures and purification procedures," *Phys. Rev. A*, vol. 57, pp. 1619–1633, Mar 1998.

[12] J. Gao, L.-F. Qiao, Z.-Q. Jiao, Y.-C. Ma, C.-Q. Hu, R.-J. Ren, A.-L. Yang, H. Tang, M.-H. Yung, and X.-M. Jin, "Experimental machine learning of quantum states," *Phys. Rev. Lett.*, vol. 120, p. 240501, Jun 2018.

[13] O. Gühne and G. Tóth, "Entanglement detection," *Physics Reports*, vol. 474, no. 1-6, pp. 1–75, 2009.

[14] J. Řeháček, B.-G. Englert, and D. Kaszlikowski, "Minimal qubit tomography," *Phys. Rev. A*, vol. 70, p. 052321, Nov 2004.

[15] K. Życzkowski, P. Horodecki, A. Sanpera, and M. Lewenstein, "Volume of the set of separable states," *Phys. Rev. A*, vol. 58, pp. 883–892, Aug 1998.

[16] A. S. Cacciapuoti, M. Caleffi, F. Tafuri, F. S. Cataliotti, S. Gherardini, and G. Bianchi, "Quantum internet: networking challenges in distributed quantum computing," *IEEE Network*, vol. 34, no. 1, pp. 137–143, 2019.

[17] M. Pant, H. Krovi, D. Towsley, L. Tassiulas, L. Jiang, P. Basu, D. Englund, and S. Guha, "Routing entanglement in the quantum internet," *npj Quantum Information*, vol. 5, no. 1, pp. 1–9, 2019.

[18] R. Fortes and G. Rigolin, "Fighting noise with noise in realistic quantum teleportation," *Phys. Rev. A*, vol. 92, p. 012338, Jul 2015.

[19] J.-S. Xu, M.-H. Yung, X.-Y. Xu, J.-S. Tang, C.-F. Li, and G.-C. Guo, "Robust bidirectional links for photonic quantum networks," *Science advances*, vol. 2, no. 1, p. e1500672, 2016.

[20] J. Schulman, F. Wolski, P. Dhariwal, A. Radford, and O. Klimov, "Proximal policy optimization algorithms," *arXiv:1707.06347*, 2017.

[21] Y. Yuan, Y. Zhao, B. Zong, and S. Parolari, "Potential key technologies for 6g mobile communications," *Science China Information Sciences*, vol. 63, no. 8, pp. 1–19, 2020.

[22] E. Schrödinger, "Discussion of probability relations between separated systems," *Mathematical Proceedings of the Cambridge Philosophical Society*, vol. 31, no. 4, p. 555–563, 1935.

[23] A. Einstein, B. Podolsky, and N. Rosen, "Can quantum-mechanical description of physical reality be considered complete?," *Phys. Rev.*, vol. 47, pp. 777–780, May 1935.

[24] M. B. Plenio and S. Virmani, "An introduction to entanglement theory," in *Quantum Information and Coherence*, pp. 173–209, Springer, 2014.

[25] R. Horodecki, P. Horodecki, M. Horodecki, and K. Horodecki, "Quantum entanglement," *Rev. Mod. Phys.*, vol. 81, pp. 865–942, Jun 2009.

[26] F. Mintert, A. Carvalho, M. Kuś, and A. Buchleitner, "Measures and dynamics of entangled states," *Physics Reports*, vol. 415, no. 4, pp. 207 – 259, 2005.

[27] A. Steane, "Quantum computing," *Reports on Progress in Physics*, vol. 61, pp. 117–173, feb 1998.

[28] D. Bouwmeester, J.-W. Pan, K. Mattle, M. Eibl, H. Weinfurter, and A. Zeilinger, "Experimental quantum teleportation," *Nature*, vol. 390, pp. 575–579, Dec 1997.

[29] A. Salles, F. de Melo, M. P. Almeida, M. Hor-Meyll, S. P. Walborn, P. H. Souto Ribeiro, and L. Davidovich, "Experimental investigation of the dynamics of entanglement: Sudden death, complementarity, and continuous monitoring of the environment," *Phys. Rev. A*, vol. 78, p. 022322, Aug 2008.

[30] K. Bartkiewicz, B. Horst, K. Lemr, and A. Miranowicz, "Entanglement estimation from Bell inequality violation," *Phys. Rev. A*, vol. 88, p. 052105, Nov 2013.

[31] P. Horodecki, "From limits of quantum operations to multicopy entanglement witnesses and state-spectrum estimation," *Phys. Rev. A*, vol. 68, p. 052101, Nov 2003.

[32] F. A. Bovino, G. Castagnoli, A. Ekert, P. Horodecki, C. M. Alves, and A. V. Sergienko, "Direct measurement of nonlinear properties of bipartite quantum states," *Phys. Rev. Lett.*, vol. 95, p. 240407, Dec 2005.

[33] A. R. R. Carvalho, F. Mintert, and A. Buchleitner, "Decoherence and multipartite entanglement," *Phys. Rev. Lett.*, vol. 93, p. 230501, Dec 2004.

[34] Z.-H. Chen, Z.-H. Ma, O. Gühne, and S. Severini, "Estimating entanglement monotones with a generalization of the Wootters formula," *Phys. Rev. Lett.*, vol. 109, p. 200503, Nov 2012.

[35] L. Aolita and F. Mintert, "Measuring multipartite concurrence with a single factorizable observable," *Phys. Rev. Lett.*, vol. 97, p. 050501, Aug 2006.

[36] S. P. Walborn, P. H. Souto Ribeiro, L. Davidovich, F. Mintert, and A. Buchleitner, "Experimental determination of entanglement with a single measurement," *Nature*, vol. 440, pp. 1022–1024, Apr 2006.

[37] P. Badziąg, i. c. v. Brukner, W. Laskowski, T. Paterek, and M. Żukowski, "Experimentally friendly geometrical criteria for entanglement," *Phys. Rev. Lett.*, vol. 100, p. 140403, Apr 2008.

[38] M. Huber, F. Mintert, A. Gabriel, and B. C. Hiesmayr, "Detection of high-dimensional genuine multipartite entanglement of mixed states," *Phys. Rev. Lett.*, vol. 104, p. 210501, May 2010.

[39] O. Gühne, M. Reimpell, and R. F. Werner, "Estimating entanglement measures in experiments," *Phys. Rev. Lett.*, vol. 98, p. 110502, Mar 2007.

[40] J. Eisert, F. G. S. L. Brandão, and K. M. R. Audenaert, "Quantitative entanglement witnesses," *New Journal of Physics*, vol. 9, pp. 46–46, mar 2007.

[41] R. Augusiak, M. Demianowicz, and P. Horodecki, "Universal observable detecting all two-qubit entanglement and determinant-based separability tests," *Phys. Rev. A*, vol. 77, p. 030301, Mar 2008.

[42] A. Osterloh and P. Hyllus, "Estimating multipartite entanglement measures," *Phys. Rev. A*, vol. 81, p. 022307, Feb 2010.

[43] L. Rudnicki, P. Horodecki, and K. Życzkowski, "Collective uncertainty entanglement test," *Phys. Rev. Lett.*, vol. 107, p. 150502, Oct 2011.

[44] B. Jungnitsch, T. Moroder, and O. Gühne, "Taming multiparticle entanglement," *Phys. Rev. Lett.*, vol. 106, p. 190502, May 2011.

[45] L. Rudnicki, Z. Puchała, P. Horodecki, and K. Życzkowski, "Collectibility for mixed quantum states," *Phys. Rev. A*, vol. 86, p. 062329, Dec 2012.

[46] Ł. Rudnicki, Z. Puchała, P. Horodecki, and K. Życzkowski, "Constructive entanglement test from triangle inequality," *Journal of Physics A: Mathematical and Theoretical*, vol. 47, p. 424035, oct 2014.

[47] L. Zhou and Y.-B. Sheng, "Detection of nonlocal atomic entanglement assisted by single photons," *Phys. Rev. A*, vol. 90, p. 024301, Aug 2014.

[48] H. S. Park, S.-S. B. Lee, H. Kim, S.-K. Choi, and H.-S. Sim, "Construction of an optimal witness for unknown two-qubit entanglement," *Phys. Rev. Lett.*, vol. 105, p. 230404, Dec 2010.

[49] W. Laskowski, D. Richart, C. Schwemmer, T. Paterek, and H. Weinfurter, "Experimental Schmidt decomposition and state independent entanglement detection," *Phys. Rev. Lett.*, vol. 108, p. 240501, Jun 2012.

[50] Y.-C. Ma and M.-H. Yung, "Transforming Bell's inequalities into state classifiers with machine learning," *npj Quantum Information*, vol. 4, p. 34, Jul 2018.

[51] S. Lu, S. Huang, K. Li, J. Li, J. Chen, D. Lu, Z. Ji, Y. Shen, D. Zhou, and B. Zeng, "Separability-entanglement classifier via machine learning," *Phys. Rev. A*, vol. 98, p. 012315, Jul 2018.

[52] C. H. Bennett, D. P. DiVincenzo, J. A. Smolin, and W. K. Wootters, "Mixed-state entanglement and quantum error correction," *Phys. Rev. A*, vol. 54, pp. 3824–3851, Nov 1996.

[53] K. Bartkiewicz, K. Lemr, A. Černoch, and A. Miranowicz, "Bell nonlocality and fully entangled fraction measured in an entanglement-swapping device without quantum state tomography," *Phys. Rev. A*, vol. 95, p. 030102, Mar 2017.

[54] A. S. M. de Castro and V. V. Dodonov, "Covariance measures of intermode correlations and inseparability for continuous variable quan-

tum systems," *Journal of Optics B: Quantum and Semiclassical Optics*, vol. 5, pp. S593–S608, oct 2003.

[55] M. Horodecki, P. Horodecki, and R. Horodecki, "Separability of mixed states: necessary and sufficient conditions," *Physics Letters A*, vol. 223, no. 1, pp. 1–8, 1996.

[56] A. Peres, "Separability criterion for density matrices," *Phys. Rev. Lett.*, vol. 77, pp. 1413–1415, Aug 1996.

[57] M. Abadi, P. Barham, J. Chen, Z. Chen, A. Davis, J. Dean, M. Devin, S. Ghemawat, G. Irving, M. Isard, *et al.*, "Tensorflow: A system for large-scale machine learning," in *12th {USENIX} symposium on operating systems design and implementation ({OSDI} 16)*, pp. 265–283, 2016.

[58] K. Lemr, K. Bartkiewicz, and A. Černoch, "Experimental measurement of collective nonlinear entanglement witness for two qubits," *Phys. Rev. A*, vol. 94, p. 052334, Nov 2016.

[59] M. A. Nielsen and I. L. Chuang, "Quantum computation and quantum information," *Phys. Today*, vol. 54, no. 2, p. 60, 2001.

[60] C. Hughes, J. Isaacson, A. Perry, R. F. Sun, and J. Turner, *Quantum computing for the quantum curious*. Springer Nature, 2021.

[61] B. C. Hiesmayr, "Free versus bound entanglement, a NP-hard problem tackled by machine learning," *Scientific Reports*, vol. 11, Oct. 2021.

[62] L. Gurvits, "Classical deterministic complexity of edmonds' problem and quantum entanglement," in *Proceedings of the thirty-fifth ACM symposium on Theory of computing - STOC '03*, ACM Press, 2003.

[63] S. Gharibian, "Strong NP-hardness of the quantum separability problem," *Quantum Information & Computation*, vol. 10, no. 3&4, p. 343–360, 2010.

[64] Y. Huang, "Computing quantum discord is NP-complete," *New Journal of Physics*, vol. 16, p. 033027, Mar. 2014.

[65] K. Bartkiewicz, A. Černoch, K. Lemr, and A. Miranowicz, "Priority choice experimental two-qubit tomography: Measuring one by one

all elements of density matrices," *Scientific Reports*, vol. 6, p. 19610, Jan 2016.

[66] M. Paris and J. Rehacek, *Quantum state estimation*, vol. 649. Springer Science & Business Media, 2004.

[67] S. Hill and W. K. Wootters, "Entanglement of a pair of quantum bits," *Physical review letters*, vol. 78, no. 26, p. 5022, 1997.

[68] V. Vedral, M. B. Plenio, M. A. Rippin, and P. L. Knight, "Quantifying entanglement," *Physical Review Letters*, vol. 78, no. 12, p. 2275, 1997.

[69] O. Gühne and N. Lütkenhaus, "Nonlinear entanglement witnesses," *Phys. Rev. Lett.*, vol. 96, p. 170502, May 2006.

[70] K. Bartkiewicz, J. c. v. Beran, K. Lemr, M. Norek, and A. Miranowicz, "Quantifying entanglement of a two-qubit system via measurable and invariant moments of its partially transposed density matrix," *Phys. Rev. A*, vol. 91, p. 022323, Feb 2015.

[71] M. Mohri, A. Rostamizadeh, and A. Talwalkar, *Foundations of machine learning*. MIT press, 2018.

[72] K. Hornik, M. Stinchcombe, and H. White, "Multilayer feedforward networks are universal approximators," *Neural networks*, vol. 2, no. 5, pp. 359–366, 1989.

[73] C. Ren and C. Chen, "Steerability detection of an arbitrary two-qubit state via machine learning," *Phys. Rev. A*, vol. 100, p. 022314, Aug 2019.

[74] Y.-Q. Zhang, L.-J. Yang, Q.-L. He, and L. Chen, "Machine learning on quantifying quantum steerability," *Quantum Information Processing*, vol. 19, no. 8, 2020.

[75] A. Canabarro, S. Brito, and R. Chaves, "Machine learning nonlocal correlations," *Phys. Rev. Lett.*, vol. 122, p. 200401, May 2019.

[76] F. F. Fanchini, G. b. u. Karpat, D. Z. Rossatto, A. Norambuena, and R. Coto, "Estimating the degree of non-markovianity using machine learning," *Phys. Rev. A*, vol. 103, p. 022425, Feb 2021.

[77] D. Koutnỳ, L. Ginés, M. Moczała-Dusanowska, S. Höfling, C. Schneider, A. Predojević, and M. Ježek, "Deep learning of quantum

entanglement from incomplete measurements," *arXiv preprint arXiv:2205.01462*, 2022.

[78] D. Gross, Y.-K. Liu, S. T. Flammia, S. Becker, and J. Eisert, "Quantum state tomography via compressed sensing," *Physical review letters*, vol. 105, no. 15, p. 150401, 2010.

[79] C. A. Riofrio, D. Gross, S. T. Flammia, T. Monz, D. Nigg, R. Blatt, and J. Eisert, "Experimental quantum compressed sensing for a seven-qubit system," *Nature communications*, vol. 8, no. 1, p. 15305, 2017.

[80] C. A. Fuchs and R. Schack, "Quantum-bayesian coherence," *Reviews of modern physics*, vol. 85, no. 4, p. 1693, 2013.

[81] D. P. Kingma and J. Ba, "Adam: A method for stochastic optimization," *arXiv preprint arXiv:1412.6980*, 2014.

[82] K. Jiráková, A. Černoch, K. Lemr, K. Bartkiewicz, and A. Miranowicz, "Experimental hierarchy and optimal robustness of quantum correlations of two-qubit states with controllable white noise," *arXiv preprint arXiv:2103.03691*, 2021.

[83] J.-W. Pan, D. Bouwmeester, H. Weinfurter, and A. Zeilinger, "Experimental entanglement swapping: Entangling photons that never interacted," *Phys. Rev. Lett.*, vol. 80, pp. 3891–3894, May 1998.

[84] V. c. v. Trávníček, K. Bartkiewicz, A. Černoch, and K. Lemr, "Experimental diagnostics of entanglement swapping by a collective entanglement test," *Phys. Rev. Applied*, vol. 14, p. 064071, Dec 2020.

[85] F. Chollet *et al.*, "Keras," 2022.

[86] S. Miyagawa, S. Ojima, R. C. Berwick, and K. Okanoya, "The integration hypothesis of human language evolution and the nature of contemporary languages," *Frontiers in psychology*, vol. 5, p. 564, 2014.

[87] M. D. Hauser, *The evolution of communication*. Cambridge, Massachusetts: MIT press, 1996.

[88] B. M. Leiner, V. G. Cerf, D. D. Clark, R. E. Kahn, L. Kleinrock, D. C. Lynch, J. Postel, L. G. Roberts, and S. Wolff, "A brief history of the internet," *ACM SIGCOMM Computer Communication Review*, vol. 39, no. 5, pp. 22–31, 2009.

[89] N. Gisin and R. Thew, "Quantum communication," *Nature photonics*, vol. 1, no. 3, pp. 165–171, 2007.

[90] C. H. Bennett and G. Brassard, "Quantum cryptography: Public key distribution and coin tossing," *arXiv preprint arXiv:2003.06557*, 2020.

[91] A. K. Ekert, "Quantum cryptography and Bell's theorem," in *Quantum Measurements in Optics*, pp. 413–418, Boston, MA: Springer, 1992.

[92] Y. Cao, Y. Zhao, Q. Wang, J. Zhang, S. X. Ng, and L. Hanzo, "The evolution of quantum key distribution networks: On the road to the qinternet," *IEEE Communications Surveys & Tutorials*, vol. 24, no. 2, pp. 839–894, 2022.

[93] M. Hillery, V. Bužek, and A. Berthiaume, "Quantum secret sharing," *Physical Review A*, vol. 59, no. 3, p. 1829, 1999.

[94] C. H. Bennett, G. Brassard, C. Crépeau, R. Jozsa, A. Peres, and W. K. Wootters, "Teleporting an unknown quantum state via dual classical and einstein-podolsky-rosen channels," *Physical review letters*, vol. 70, no. 13, p. 1895, 1993.

[95] D. Gottesman and I. L. Chuang, "Demonstrating the viability of universal quantum computation using teleportation and single-qubit operations," *Nature*, vol. 402, no. 6760, pp. 390–393, 1999.

[96] H. J. Kimble, "The quantum internet," *Nature*, vol. 453, no. 7198, pp. 1023–1030, 2008.

[97] L. Gyongyosi and S. Imre, "Advances in the quantum internet," *Communications of the ACM*, vol. 65, no. 8, pp. 52–63, 2022.

[98] S. Wehner, D. Elkouss, and R. Hanson, "Quantum internet: A vision for the road ahead," *Science*, vol. 362, no. 6412, p. eaam9288, 2018.

[99] A. Singh, K. Dev, H. Siljak, H. D. Joshi, and M. Magarini, "Quantum internet—applications, functionalities, enabling technologies, challenges, and research directions," *IEEE Communications Surveys & Tutorials*, vol. 23, no. 4, pp. 2218–2247, 2021.

[100] L. Gyongyosi and S. Imre, "Topology adaption for the quantum internet," *Quantum Information Processing*, vol. 17, no. 11, pp. 1–12, 2018.

[101] K. Goodenough, D. Elkouss, and S. Wehner, "Optimizing repeater schemes for the quantum internet," *Physical Review A*, vol. 103, no. 3, p. 032610, 2021.

[102] W. J. Munro, Y.-H. Luo, M.-C. Chen, M. Erhard, H.-S. Zhong, D. Wu, H.-Y. Tang, Q. Zhao, X.-L. Wang, K. Fujii, *et al.*, "Teleportation in quantum edge networks (conference presentation)," in *Quantum Communications and Quantum Imaging XX*, p. PC122380G, SPIE, 2022.

[103] H.-J. Briegel, W. Dür, J. I. Cirac, and P. Zoller, "Quantum repeaters: the role of imperfect local operations in quantum communication," *Physical Review Letters*, vol. 81, no. 26, p. 5932, 1998.

[104] B. Jacobs, T. Pittman, and J. Franson, "Quantum relays and noise suppression using linear optics," *Physical Review A*, vol. 66, no. 5, p. 052307, 2002.

[105] L. Fu, D. Sun, and L. R. Rilett, "Heuristic shortest path algorithms for transportation applications: State of the art," *Computers & Operations Research*, vol. 33, no. 11, pp. 3324–3343, 2006.

[106] K. Mattle, H. Weinfurter, P. G. Kwiat, and A. Zeilinger, "Dense coding in experimental quantum communication," *Physical Review Letters*, vol. 76, no. 25, p. 4656, 1996.

[107] M. Horodecki, P. Horodecki, and R. Horodecki, "General teleportation channel, singlet fraction, and quasidistillation," *Physical Review A*, vol. 60, no. 3, p. 1888, 1999.

[108] K. Mehlhorn, P. Sanders, and P. Sanders, *Algorithms and data structures: The basic toolbox*, vol. 55. Berlin: Springer, 2008.

[109] R. Bellman, "On a routing problem," *Quarterly of applied mathematics*, vol. 16, no. 1, pp. 87–90, 1958.

[110] P. E. Hart, N. J. Nilsson, and B. Raphael, "A formal basis for the heuristic determination of minimum cost paths," *IEEE transactions on Systems Science and Cybernetics*, vol. 4, no. 2, pp. 100–107, 1968.

[111] A. Raffin, A. Hill, A. Gleave, A. Kanervisto, M. Ernestus, and N. Dormann, "Stable-baselines3: Reliable reinforcement learning implementations," *Journal of Machine Learning Research*, 2021.

Apendix

Faculty
of Science

Confirmation of contribution

As the supervisor to Mgr. Jan Roik and corresponding author of his publications

[1] J. Roik, K. Bartkiewicz, A. Černoch, and K. Lemr, "Accuracy of entanglement detection via artificial neural networks and human-designed entanglement witnesses," Phys. Rev. Appl. **15**, 054006 (2021),

[2] J. Roik, K. Bartkiewicz, A. Černoch, and K. Lemr, "Entanglement quantification from collective measurements processed by machine learning," Phys. Lett. A **446**, 128270 (2022),

[3] J. Roik, K. Bartkiewicz, A. Černoch, and K. Lemr, "Routing in quantum communications networks using reinforcement machine learning," submitted (2023)

I hereby certify that Mgr. Jan Roik significantly contributed to the scientific investigation presented in these publications. Typically, he programmed the machine learning models, evaluated obtained data and dominantly contributed to writing of the manuscripts. Extracts of the publications directly quoted in his thesis are of his own writing.

Olomouc, 6th March 2023 .....

doc. Mgr. Karel Lemr, Ph.D.
Joint Laboratory of Optics

Palacký University Olomouc | Faculty of Science
17. listopadu1192/12 | CZ 771 46 Olomouc | Czech Republic | T: +420 585 634 060
www.prf.upol.cz

Faculty
of Science

Genius loci ...

Confirmation of contribution

As the co-author of Mgr. Jan Roik publications:

[1] J. Roık, K. Bartkıewıcz, A. Cernoch, and K. Lemr, "Accuracy of entanglement detection via artificial neural networks and human-designed entanglement witnesses," Phys. Rev. Appl. 15, 054006 (2021),

[2] J. Roik, K. Bartkiewicz, A. Černoch, and K. Lemr, "Entanglement quantification from collective measurements processed by machine learning," Phys. Lett. A 446, 128270 (2022),

[3] J. Roik, K. Bartkiewicz, A. Černoch, and K. Lemr, "Routing in quantum communications networks using reinforcement machine learning," submitted (2023)

I hereby certify that Mgr. Jan Roik significantly contributed to the scientific investigation presented in these publications. Typically, he programmed the machine learning models, evaluated obtained data and dominantly contributed to writing of the manuscripts. Extracts of the publications directly quoted in his thesis are of his own writing.

Olomouc, 6th March 2023 .....

Mgr. Antonín Černoch, Ph.D.
Joint Laboratory of Optics

ADAM MICKIEWICZ UNIVERSITY, POZNAŃ
Faculty of Physics, Institute of Spintronics and Quantum Information

6.03.2023, Poznań

To whom it may concern,

I declare that Mgr. Jan Roik contributed significantly to the scientific research presented in the publications [1,2,3]. His contributions included implementing and applying artificial intelligence methods to solve the particular research tasks, processing the obtained data, and dominantly contributing to the writing of manuscripts. He wrote the extracts of the publications quoted directly in his thesis.

[1] J. Roik, K. Bartkiewicz, A. Černoch, and K. Lemr, "Accuracy of entanglement detection via artificial neural networks and human-designed entanglement witnesses," Physical Review Applied, vol. 15, no. 5, p.054006, 2021.

[2] J. Roik, K. Bartkiewicz, A. Černoch, and K. Lemr, "Entanglement quantification from collective measurements processed by machine learning," Physics Letters A, vol. 446, p. 128270, 2022.

[3] J. Roik, K. Bartkiewicz, A. Černoch, and K. Lemr, "Routing in quantum communications networks using reinforcement machine learning," MANUSCRIPT SUBMITTED FOR PUBLICATION, 2023.

K. Bartkiewicz

Prof. UAM dr hab. Karol Bartkiewicz

ul. Uniwersytetu Poznańskiego 2, 61-614 Poznań, Poland
tel. +48 61 829 5236
e-mail bark@amu.edu.pl
www.amu.edu.pl